AD-786 232

HIGH POWER DYE LASERS

UNITED AIRCRAFT RESEARCH LABORATORIES

PREPARED FOR
OFFICE OF NAVAL RESEARCH
ADVANCED RESEARCH PROJECTS AGENCY

30 SEPTEMBER 1974

REPORT DOCUMENTATION PAGE		READ INSTRUCTIONS BEFORE COMPLETING FORM
1. REPORT NUMBER N921617-8	2. GOVT ACCESSION NO.	3. RECIPIENT'S CATALOG NUMBER **AD-786 232**
4. TITLE (and Subtitle) HIGH POWER DYE LASERS		5. TYPE OF REPORT & PERIOD COVERED Annual Technical 3/1/74 - 9/30/74
		6. PERFORMING ORG. REPORT NUMBER N921617-8
7. AUTHOR(s) Morey, W. W. & Glenn, W. H.		8. CONTRACT OR GRANT NUMBER(s) N00014-73-C-0284
9. PERFORMING ORGANIZATION NAME AND ADDRESS United Aircraft Research Laboratories 400 Main Street East Hartford, Conn. 06108		10. PROGRAM ELEMENT, PROJECT, TASK AREA & WORK UNIT NUMBERS ARPA
11. CONTROLLING OFFICE NAME AND ADDRESS Office of Naval Research Department of Navy Arlington, VA 22217		12. REPORT DATE 9/30/74
		13. NUMBER OF PAGES 54
14. MONITORING AGENCY NAME & ADDRESS(if different from Controlling Office) Director, Physics Programs Physical Sciences Division Office of Naval Research 800 N. Quincy Street, Arlington, VA 22217		15. SECURITY CLASS. (of this report) Unclassified
		15a. DECLASSIFICATION DOWNGRADING SCHEDULE

16. DISTRIBUTION STATEMENT (of this Report)

Approved for public release, distribution unlimited

17. DISTRIBUTION STATEMENT (of the abstract entered in Block 20, if different from Report)

18. SUPPLEMENTARY NOTES

19. KEY WORDS (Continue on reverse side if necessary and identify by block number)

High Power Dye Lasers
Flashlamps

20. ABSTRACT (Continue on reverse side if necessary and identify by block number)

This report describes modifications made to the previously reported high power dye laser to allow for increased power handling capability, repetition rate and operating times. The redesigned flashlamp has been operated at power levels over 50 kW and at repetition rates up to 500 Hz. Present problem are primarily involved with dye circulation and heat dissipation and the solution to these should lead to powers output from the dye laser that are well in excess of the presently available level of 41 watts.

DD FORM 1 JAN 73 1473 EDITION OF 1 NOV 65 IS OBSOLETE

UNITED AIRCRAFT CORPORATION
RESEARCH LABORATORIES

Report Number: N-921617-8
Semi-Annual Technical Report for the period
1 March 1974 to 30 September 1974

HIGH POWER DYE LASERS

UNITED AIRCRAFT RESEARCH LABORATORIES

SEMI-ANNUAL REPORT N921617-8

TABLE OF CONTENTS

SECTION I

INTRODUCTION AND TECHNICAL REPORT SUMMARY

At the end of the last reporting period 39 watts of average laser power was obtained from the dye laser by driving the flashlamp with a rotary spark gap whose operation has been described recently in the literature by C. M. Ferrar (Ref. 1). The rotary spark gap eliminated the problem of deionization of the gap between flashlamp shots that previously limited the lamp to repetition rates of about 30 Hz. Repetition rates well over a 100 Hz were easily demonstrated with the rotary gap; and, in addition, the rotary gap can easily handle the large peak current requirements (15 kA) and repetition rate for which a long lived hydrogen thyratron is commerically unavailable. Short term operation of the laser was required even for laser outputs less than 39 watts average power due to the severe heat loading on the electrodes, the fused quartz envelope, and the gas exhaust tubes and plenums. In addition, the third triggering electrode which was thermally insulated and exposed to the hot arc plasma would have deteriorated rapidly if the laser was run on a longer term basis. As a consequence, during the period of the present report the flashlamp was redesigned to allow water cooling of both electrodes and the fused quartz envelope and to allow for convenient disassembly to examine, repair, or clean the various components of the lamp a feature the previous lamp did not have. The third triggering electrode that had extended up through the center of the cathode of the previous version of the flashlamp was eliminated and replaced by sustainer discharge that runs continuously between the lamp electrodes and that is electrically in series with the rotary spark gap and capacitor. The sustainer, which is a low current dc discharge of a few milliamperes, was described in the last report in connection with the unconfined vortex arc tests. The flashlamp system now operates in the following manner: When the electrodes of the rotary spark gap come into near proximaty the capacitor self discharges through the rotary gap and the sustainer glow discharge that is stabilized on the interelectrode axis by the vortex flow in the lamp housing.

A more rugged rotary spark gap with 4 electrodes on the rotating disc was also constructed that would allow for a longer electrode life and repetition rates up to 800 Hz. The capacitor was set vertically to avoid oil leaks and a low inductance strip line connects the capacitor, spark gap, and arc lamp housing together. The laser system except for the dye pump and filter, power supply, and control rack is shown in the photograph of Figure 1. The mechanical design details of the lamp and spark gap will be discussed further in sections III and V. The power supply driving the flashlamp was previously limited to about 22 kW average power because of

UARL HIGH POWER DYE LASER

FIG. I

its slow response in charging the capacitor between lamp firings. This has since been extended to about 80 kW by modification in the wiring of the high voltage transformer.

The new high power flashlamp was tested at various pulse energies and repetition rates. On a single pulse basis 300 J has been discharged repeatedly in the lamp with no envelope damage. At repetition rates the lamp was run briefly at 255 Hz with 200 J per pulse or 51 kW input. With 10 and 15 kW input (100 and 150 J per pulse at 100 Hz) the lamp was run frequently for durations of over 2 minutes which is enough time to allow the lamp to thermally stabilize. In this instance no water cooling provisions had been provided for the fused quartz envelope. It was assumed prior to these test that the incoming gas flow at 5 ℓ/sec (STP) would be sufficient to cool the lamp envelope. The envelope, however, heated to glowing red heat ($800-900^\circ$C) that was observed when the lamp was suddenly shut off. The lamp has been recently been modified to include a fused quartz water cooling jacket surrounding the envelope. This should adequately cool the lamp to allow long term continuous operation at several tens of kilowatts. The cooling jacket will also provide increased resistance to vibration and mechanical shock from the discharge. The vibration of the envelope from discharging the flashlamp was examined and it was determined that the build up of a resonant vibration that would cause destruction during repetition rate operation was unlikely. One lamp envelope did explode, however, possibly for another reason when the pulse repetition frequency (PRF) was slowing being reduced below 100 Hz.

The absolute spectral irradiance of the flashlamp at 1 meter distance from the arc was also measured. Using these measurements we could determine the total radiance of the lamp and the electrical to optical efficiency for that part of the spectrum transmitted by the fused quartz envelope. Then, from a measurement of the exiting gas temperature taken with a thermo couple placed just above the outlet of the anode, we could determine the electrical energy that goes into the internal energy of the gas. With this data, and using a thermodynamic analysis, we could approximate the energy used for expanding the gas. The energy per shot or average power input to the lamp was then found to be divided accordingly: 14% for radiation transmitted by the lamp envelope; 37% for internal energy in the gas; and 37% for the expansion of the gas. This leaves about 12% for the i^2R losses of the spark gap and lamp electrodes and light losses at the spark gap electrode. In addition, we must include in the extra 12% the heat carried away by convection on the outside surfaces of the lamp and a small amount of power for production of sound waves that can be disagreeably loud to an unprotected listener. These measurements and calculations are further

discussed in Sections III and IV. The flashlamp also operated without difficulty at a PRF of 500 Hz with 50J per pulse; and there is no reason at this time not to expect that the lamp should operate conveniently at PRFs over 1 kHz. A ray tracing program was developed during this reporting period that defines the optical power density distribution in the dye cell region with the spherical pumping cavity. The program considers the arc as a Lambertian emmiter and allows for such things as Fresnel losses at the dye cell. Results from the ray tracing program indicate the optimum choice of dye cell diameter for maximum laser output. These results are discussed in detail in section VI of the report.

Results from the last reporting period demonstrated that the average laser output power is proportional to the PRF of the flashlamp (or electrical input power) for PRFs up to 50 Hz. As the PRF is increased beyond 50 Hz the laser power did not contiue to rise as fast as the input power and after 100 Hz the laser power actually decreased with increasing PRF. The principal cause of the fall-off in laser power is the inability of the flowing dye solution to cool the walls of the dye cell sufficiently between flashlamp firings. For ethanol, the solvent used in the above test, even a few degrees temperature differential between the cell wall and incoming dye solution can produce severe thermo-optic distortion in an optical path expanding the length of the dye cell. During this reporting period a new dye solution pumping system was assembled that has a pumping capacity over three times as great as the one used previously. Unfortunately, this did not solve the laser power fall off with increasing PRF. We observed instead the onset of cavitation with ethanol both visually and audibly in the dye cell at flow rates of 0.45 to 0.63 1/sec. These were the typical flow rates used previously. The cavitation bubbles appeared on the side of the dye cell and near the bottom end at only two places except in certain instances at higher flow rates of about 1 ℓ/sec when a vortex cavitation would occur in the middle of the cye cell. Once the onset of cavitation was reached the severity of the cavitation and the optical distortion that it caused would increase with increasing flow rate. The optical distortion from the cavitation effects nullified the improvement hoped for with the increased pumping capacity.

Average laser output power measurements taken with the new flashlamp and pumping system with flow rates at about the onset of cavitation gave results similar to that obtained previously with respect to the decrease in the laser output for PRFs greater than 100 Hz. A higher laser efficiency was obtained at the lower repetition rates, however, with the use of dissolved oxygen in the dye solution. For instance with 5 kW input at 100J per pulse 20.5 watts of laser output was obtained at a PRF of 50 Hz for an efficiency 0.4%. For the 100 J per pulse the laser output reached a maximum at 29 watts when the PRF was increased to 100 Hz and then decreased

for higher PRFs. With 200 J per pulse input the highest laser power achieved was 41 watts with a PRF of 99 Hz. The measurements taken on the dye flow system and laser power are presented and discussed in more detail in Section VII.
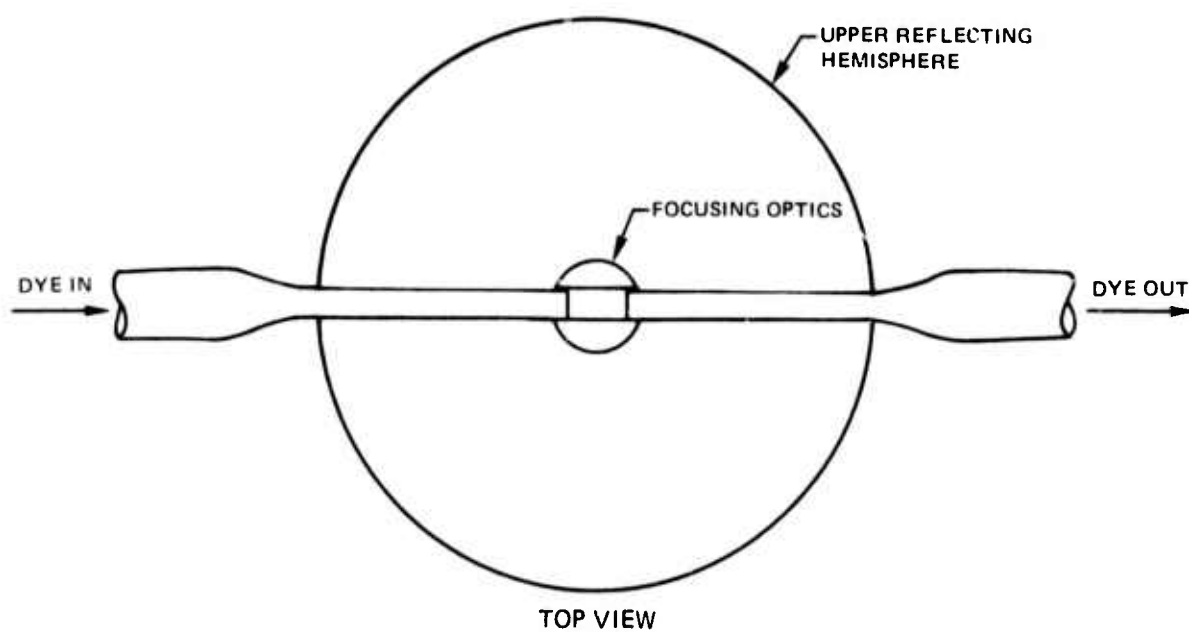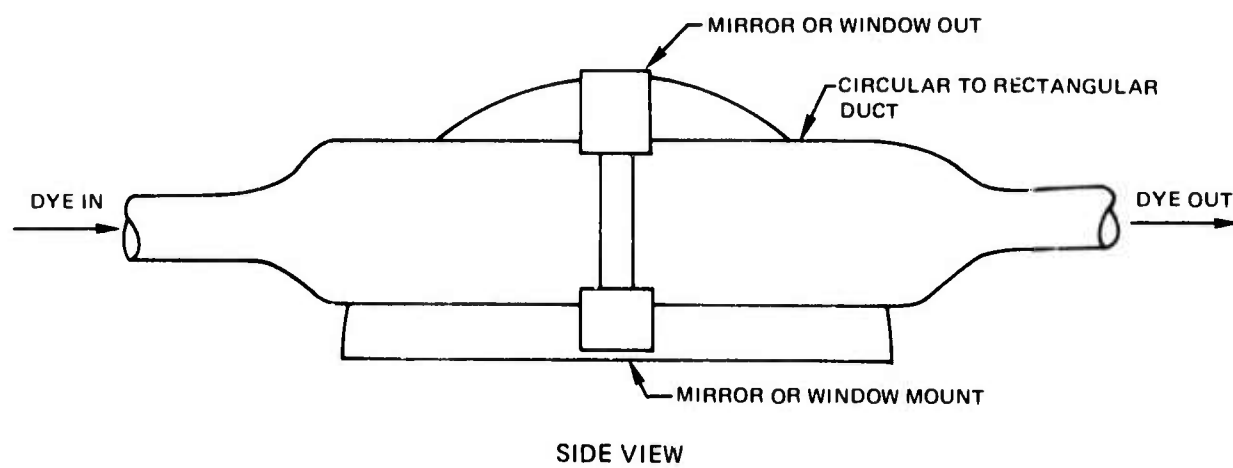
SECTION II

FUTURE DIRECTION AND RESEARCH ON HIGH POWER DYE LASER

If we could extend the 0.4% laser efficiency that we got with the 5 kW input power to the 50 kW input level at which the lamp is capable of running, we would obtain 200 watts of laser power. As mentioned in Section I, this was not possible because of the thermo-optic distortion generated in the ethanol dye solution by the heat loading from the flashlamp. Increasing the dye solution flow rate produced a faster change over rate in the dye cell and improves dye cell wall cooling. It was found, however, that this caused cavitation bubbles to form in the optical path of the dye cell. As a first priority for the coming report period, then, we will examine new solutions and techniques that will alleviate the thermo-optic distortion and cavitation in the dye cell. We will test solvents other than pure ethanol and mixtures of solvents with smaller dn/dT and larger thermal conductivities in order to maximize the average laser power. A new dye cell whose inside surface has been ground to a course finish will be tested soon with the goal of obtaining better wall cooling with the increased surface area. A sapphire dye cell is presently on order and should definitely improve the repetition rate performance of the laser due to the improved thermal conductivity of sapphire over the fused quartz presently used for the dye cell. The flow system will be studied and redesigned with fluid dynamic considerations for the reduction of turbulence in those areas that produce cavitation. By optimizing the aforementioned parameters we should be able to improve significantly upon the present 41 watts of laser power.

To approach the 200 watt potential of the laser that would be obtainable with repetition rates over 200 Hz, however, a more radical change in the dye cell system will probably be required. One approach that will be investigated during the next reporting period is a transverse flow system that pumps the dye solution across the length of the focussed arc light rather than longitudinally along the length of the focal region as it is presently done. For the same velocity of flow, the transverse geometry would change the volume of the dye in the focussed light region 7.5 times faster than in the longitudinal geometry. This, of course, for the same dye cell volume would require 7.5 times the volume flow rate. The volume of the dye cell, however, could be conveniently reduced in the transverse geometry since this geometry has inherently more flow conductance. Figure 2 shows a schematic of a possible transverse flow system that could be fitted into the existing reflecting hemispheres. The input and output ducts in the transverse flow system would block or shadow an additional amount of arc light from reaching the dye cell over what the longitudinal flow system presently shadows. This loss in optical pumping efficiency which may be 10-25% would have to be made up by improvement in laser output

FIG. 2

TRANSVERSE DYE FLOW CELL

MIRROR OR WINDOW OUT

CIRCULAR TO RECTANGULAR DUCT

DYE IN

DYE OUT

MIRROR OR WINDOW MOUNT

SIDE VIEW

UPPER REFLECTING HEMISPHERE

FOCUSING OPTICS

DYE IN

DYE OUT

TOP VIEW

-7-

N09—162—2

at repetition rate operation. In addition, some form of focusing optics or a special cell design would have to be incorporated in the transverse system to avoid severe Fresnel losses for light rays approaching the active dye flow region at small angles.

Another dye flow system that will be considered is a free flowing stream. By completely eliminating the dye cell wall we could produce a vertical stream that flows from a nozzle at the top to a funnel at the bottom. A principal problem with this system is the turbulent boundary that would be produced in the most fluids at the flow speeds desired. There are long chain molecular additives, however, that significantly reduce the turbulence of a flowing solution. Moreover, it may not be necessary to have an extremely fast flow for the free stream since this system would require only one change in the active region per laser shot. At present, for example, it takes approximately 4 changes per laser shot to bring the cell wall and dye solution to a close enough temperature to avoid severe optical degradation. A small test facility will be set up and different solutions with friction reducing additives will be examined to see if this type flow system will be practical.

In order to determine if the vortex stabilized flashlamp can be scaled up to longer discharge lengths for driving even higher average power dye lasers we will design, build and test a new flashlamp with an arc length 3 to 5 times as long as the present 6 cm arc. The mechanical design of this lamp will be simplied slightly and made suitable for placement in an elliptical pumping cavity. The present 6 cm flashlamp is underdamped and the discharge oscillates for 2 to 3 periods. With the longer arc it is expected that the increase in arc resistance will give better dampening and, hence, better electrical to optical efficiency. One of the problems faced with the longer arc is the requirement for increased breakdown voltage. With a sustainer running between the electrodes, the anode is only a few thousand volts above the cathode and the rotary spark gap can easily discharge a capacitor charged to a voltage above the sum of the sustainer breakdown voltage in the gap breakdown voltage. The difficulty would lie in getting the sustainer initiated between the electrodes. This would be especially true in the 5 times longer arc and may require operaton of the lamp at reduced pressure by pumping on the gas outlets. Another approach would be to mechanically ignite the sustainer with a conductive probe that would slide on the electrode axis to decrease the gap sapcing. Once the sustainer is ignited the probe would be withdrawn to open the gap back to its original length. After the sustainer problems are solved, the lamp will first be tested on a single shot basis. Current, voltage, and light output waveforms will be studied and the electrically to optically efficiency calculated from absoulte spectral measurements. The lamp will then be run at a repetition rate only at the power levels now available (80 kW) with our present power supply.
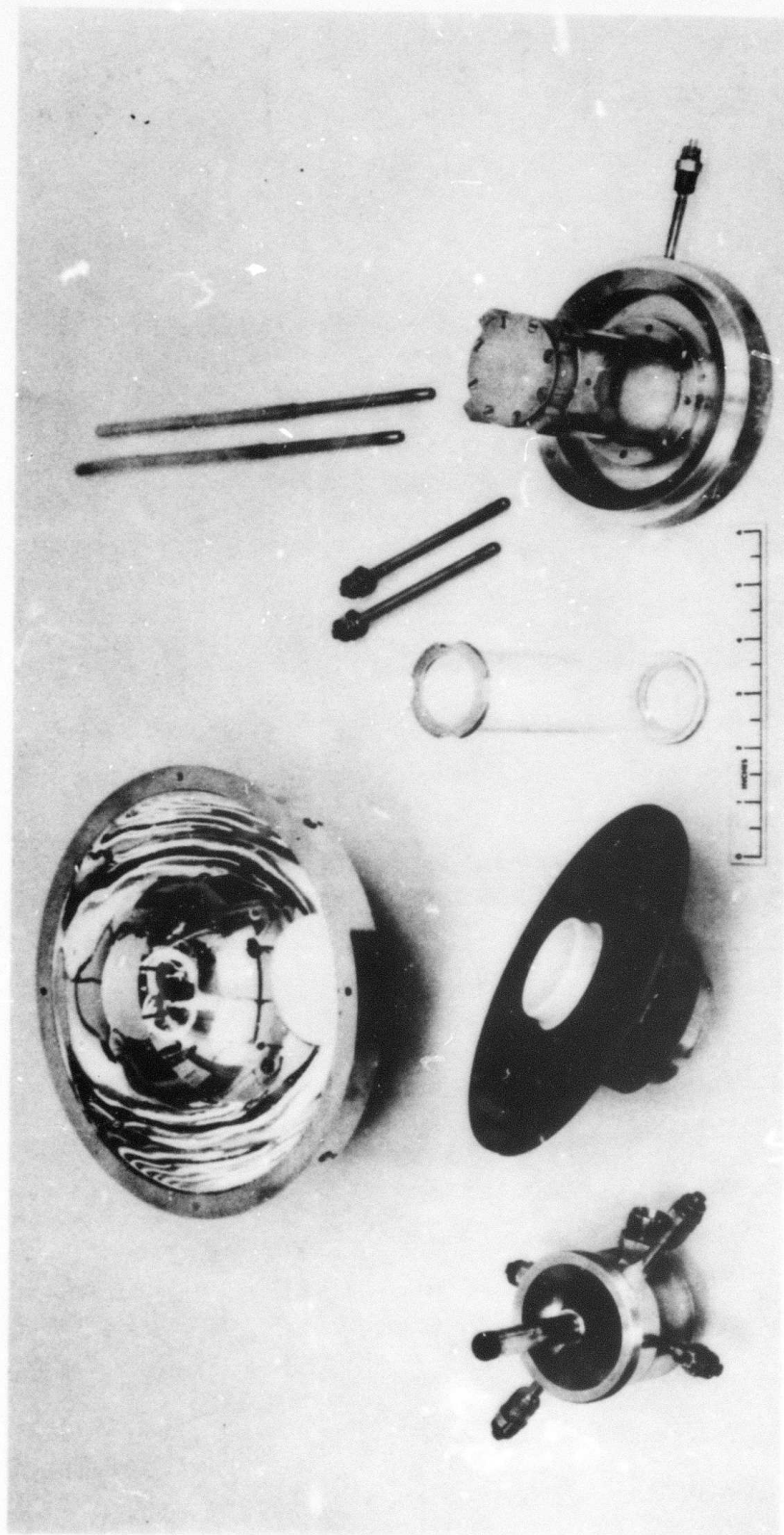
SECTION III

DESIGN AND TESTING OF NEW FLASHLAMP
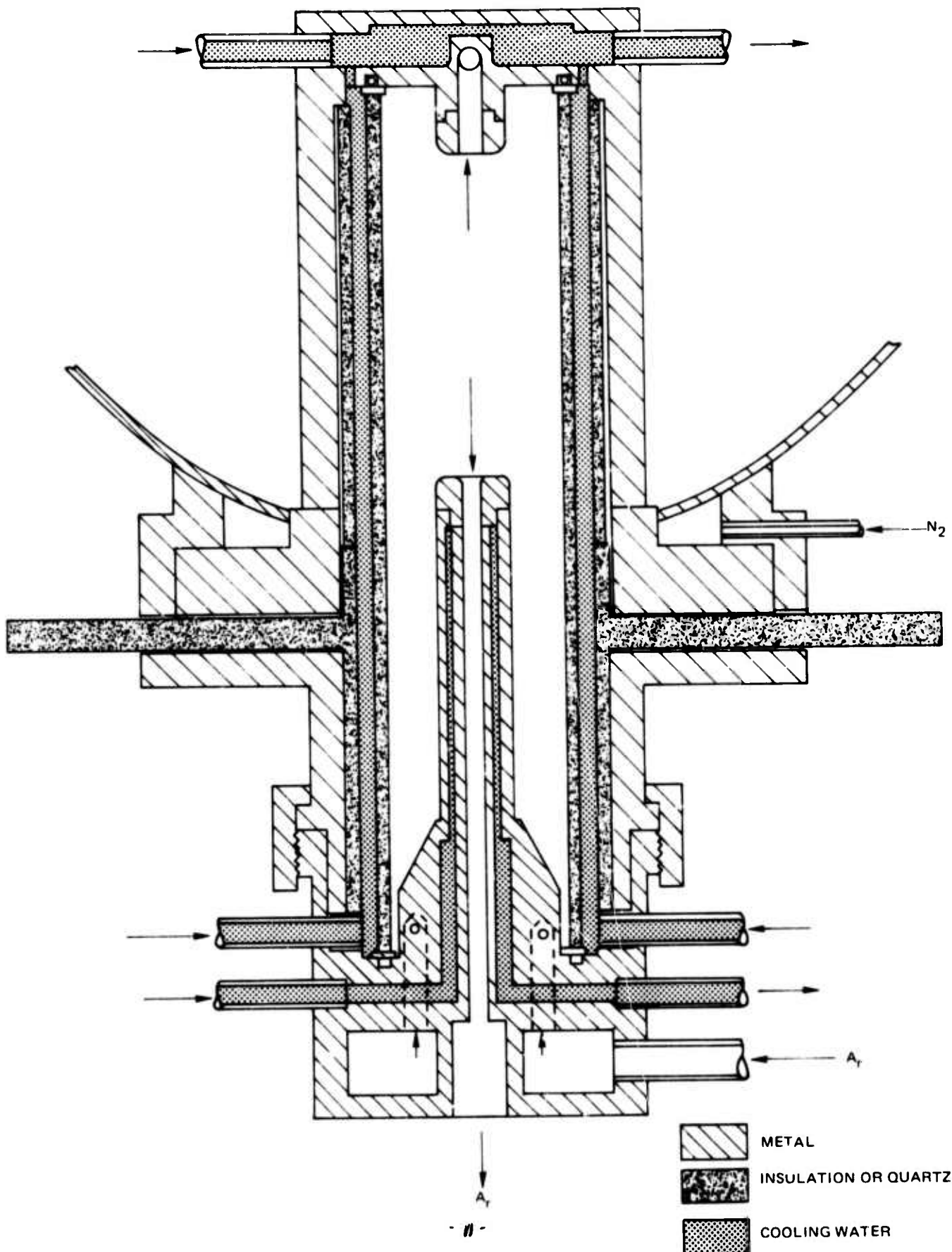
3.1 Description of Flashlamp

There were essentially two important goals in the design of the new flashlamp. One was to provide sufficiently more cooling of the electrodes to allow continuous duty operation of the lamp. The other was to build a lamp housing that could be assembled and disassembled for easy maintenance and replacement of lamp envelopes. Another consideration was to allow for the use of standard size fused quartz envelopes in place of the machine gound tolerance envelopes required previously. This later requirement was met with the use of end seals on the lamp envelope. Figure 3 shows a photograph of the flashlamp disassembled. The lower electrode housing is shown in the lower left of the photo. This housing has cooling water inlets for the lower electrode (cathode) and lamp envelope. In addition, the argon gas inlet is located at the large Swagelok connection shown. Next to the lower electrode housing is a piece consisting of an inuslating disc and alumina sleeve that are epoxied to an aluminum sleeve. This unit fits into the lower electrode housing and the two are held together with the knurled threaded ring attached to the aluminum sleeve. The lamp envelope, shown next, is made from syntheitc fused quartz (suprasil) and is compressed between "O" ring seals in the top and bottom electrode housings. The aluminum rings on the ends of the lamp envelope serve to center its position with respect to the electrodes and to protect the "O" rings from burning in the intense uv light of the lamp. The aluminum rings are sealed to the envelope with a porcelain cement and the 4 notches in the top ring allow the passage of water from the outside surface of the envelope into a chamber in the upper electrode housing. The upper electrode housing is the piece shown on the lower right hand side of the photograph. A fused quartz tube (spectrosil) that acts as a cooling jacket for the lamp envelope is cemented to the upper electrode housing structure. The cooling jacket is difficult to discern in the phosotraph, however. The lower reflecting hemisphere, also shown, connects to the upper electrode housing and is purged of air along with the upper hemisphere with nitrogen gas that enters through the connector and tube shown. All the pieces have guide rings and surfaces to keep the entire assembly concentric.

We should be safe if we allow for the water cooling to remove 85% of the input power as heat, since about 15% comes out as light. For 50 kW input this would be 10.1 kcal per second of heat removal. Considering

WATER COOLED VORTEX STABILIZED FLASHLAMP ASSEMBLY

FIG. 4

WATER COOLING FOR ARC LAMP

METAL

INSULATION OR QUARTZ

COOLING WATER

N09—162—4

a 30° temperature rise in the cooling water, we would require a flow of about .34 ℓ/sec. This flow rate, which is easily achievable with our pumping system, is an overestimate because a good portion of the input power goes into heating the gas (about 34% cf. sec. 3.5) which is then exhausted from the system. Figure 4 shows a schematic of the lamp assembly and the cooling water paths. A copper insert with the central exhaust hole for the argon was placed in the extended lower electrode to force water to flow up one side, across a channel at the top and then down the opposite side. This allows a high conductance for fast fluid flow and brings the water near the tungsten end pieces as shown. Water also flows into the bottom electrode housing and upward between the lamp envelope and insulating tube and then the fused quartz jacket to join the water flowing through the chamber in the upper electrode housing. Since deionized water is required, a closed cycle pumping system with a heat exchanger is used. The water resistance across the electrodes typically runs 5 to 10 MΩ. As contrasted with dc arc lamps that have between 5 and 8 times more heat loading on the anode than cahtode the flashlamp described here has about equal heat loading. This is due to the fact that the major heating comes from the hot arc gas rather than large $i^2 R$ losses at the electrodes. The insulating disc piece and upper electrode housing are held together tightly with two large insulating pieces and 4 spacers that act as a clamp. The insulated clamp is not shown in Fig. 3, but can be seen in Fig. 1. To assemble the lamp the upper housing and insulated disc piece are clamped together; the lamp envelope is inserted; and the lower electrode housing is fastened into place using the threaded ring to adjust the compression on the end seals of the envelope. The lower hemisphere then seats into position around the upper housing. The four tubes shown in Fig. 3, for which two carry water and the other two exhaust the argon from the upper electrode, are inserted through the hemisphere and screw into the upper housing.

3.2 Power Supply Modification

The power supply for the dye laser was built by the J. S. Betts Company and requires 220 v, 3ϕ with about 250 amperes. To obtain the current for the supply 3 step down transformers one for each phase rated at 15 kVA each was used to step down the 440 v line to 220 v. The 3ϕ power is then applied to the primary of a high voltage transformer in a delta connection through a series of powerstats connected in a wye arrangement. The powerstats permit the voltage to be set to any desired value between 0 and 20 kV. The secondary of the high voltage transformer is connected in a wye arrange-ment and drives a 3ϕ solid state bridge rectifier. When the power supply was pulse charging the flashlamp capacitor at repetition rates greater than 100 Hz it was found that the capacitor was not charging to the preset voltage. This occurred even with no ballast resistance between the power

supply and capacitor. Initially it was felt that the charging time was
wholly limited by inductive reactance. The voltage across a capacitor
that is being charged by a series R and L where the inductive reactance
is larger than the resistance is given by (Ref. 2)

$$v_c(t) = E_o \left[1 - B \exp \left\{ -(R/2L)t \right\} \sinh (kt + \theta) \right]$$

where E_o is the power supply voltage and

$$B = (R^2/4kL^2 - 1)^{\frac{1}{2}} \; ; \quad \theta = \tanh^{-1}(2kL/R)$$
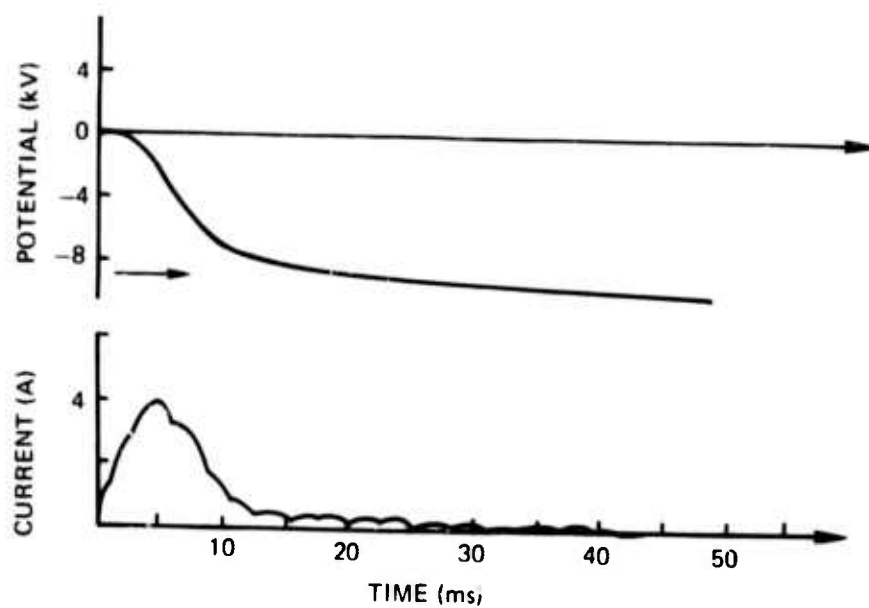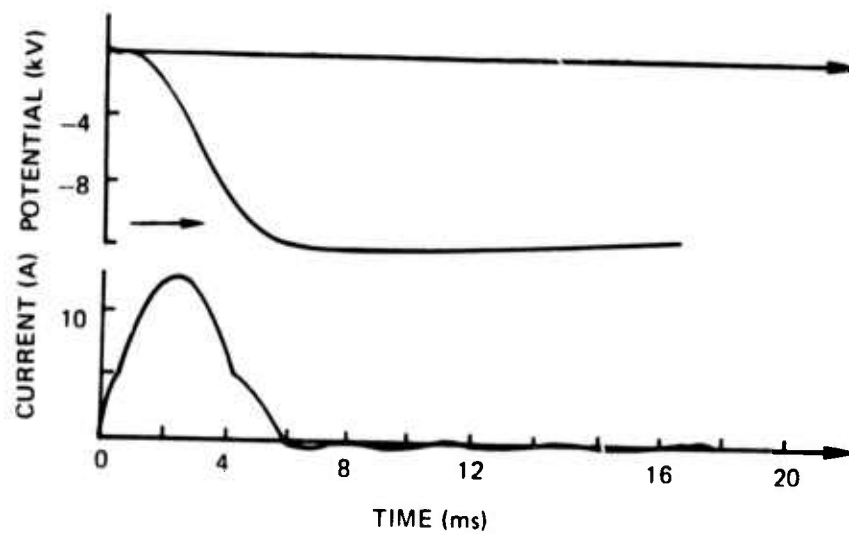
$$k = (1/LC - R^2/4L^2)^{\frac{1}{2}}$$

In this case the capacitor voltage rises above the power supply voltage and
then decays back to the power supply voltage at a much later time. Figure
5 shows the current and voltage waveforms for a single charging of the
flashlamp capacitor. The 3¢ripple can be seen on the current waveform.
The voltage waveform which is negative does not go below the supply voltage
as would be the case for reactance limited charging but instead asymptotically
approaches the supply voltage. This is probably due to the saturation of
the iron in the powerstats from the large surge current required for the
pulse charging.

The secondary of the high voltage transformer was rewired from a wye
to a delta arrangement. This reduced the maximum voltage available to 12.3 kV
and reduced the inductance of the secondary by a factor of about 2. In
addition, for voltages requirements near the maximum, the powerstat is
nearly removed from the circuit thus preventing it from limiting the
charging. Figure 5b shows the capacitor charging with the transformer
rewired. In this case, the voltage over shoots as it should with inductance
charging. Insertion of a greater portion of the powerstat into the circuit
to reduce the voltage verified its saturation effect on the charging
waveform. With the transformer modified we are limited to a charging
rate of 260 Hz to charge the capacitor to the supply voltage when the
supply is set at full voltage of 12.3 kv. Even at a reduced voltage of
10 kv we are limited only to 247 Hz for charging to the supply voltage.
Care must be taken , however, when using lower repetition rates at the higher
powerstat positions because of the overshoot of the charging voltage. The
overshooting would give one a higher input power than one might expect
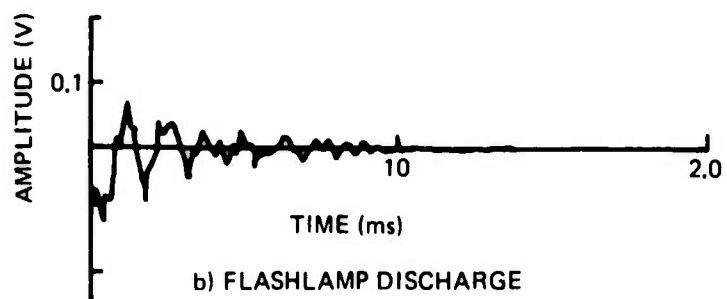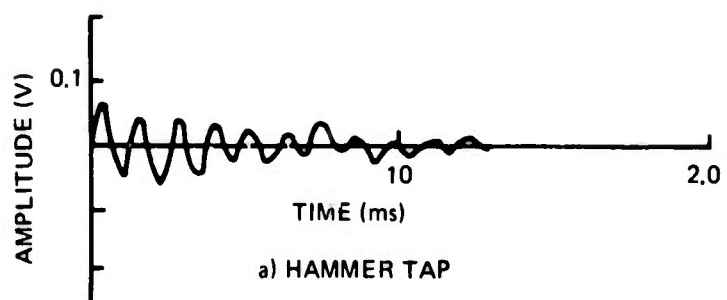otherwise.

3.3 Vibration of Lamp Envelope

The flashlamp had been operating at about 5 kW input power when the

CAPACITOR CHARGING

a) Δ–Y CONNECTION

b) Δ–Δ CONNECTION

- 14 -

ENVELOPE VIBRATION

a) HAMMER TAP
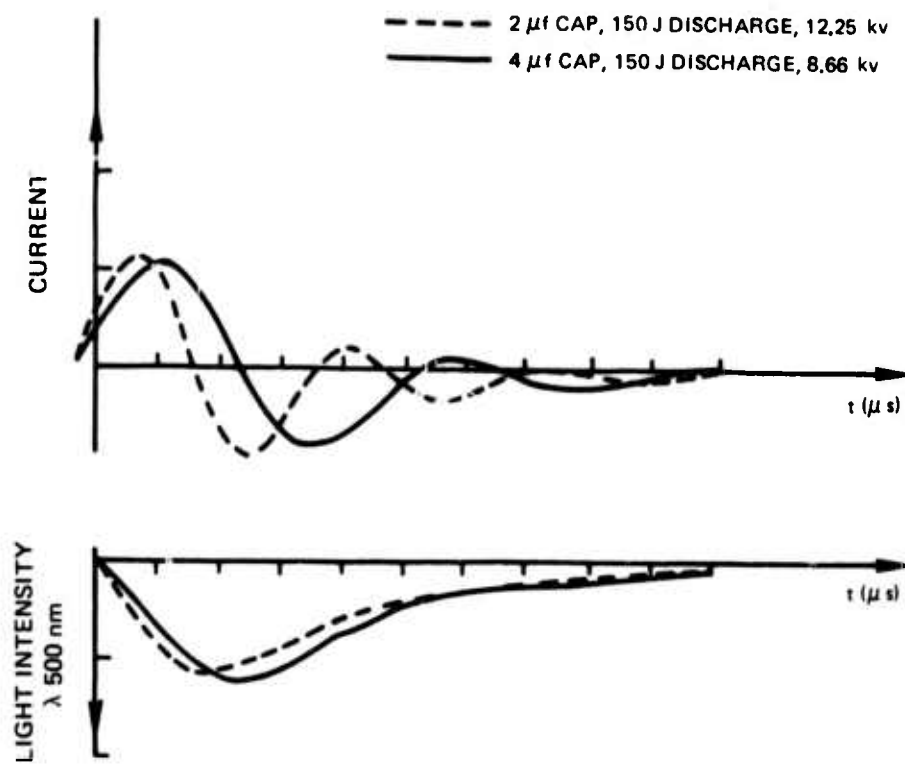
b) FLASHLAMP DISCHARGE

- 15 -

PRF was slowly decreased from a value above 100 Hz to a value a little
below 100 Hz. At this point the lamp envelope exploded. Since the input
power level was not excessive, this led us to suspect that a resonant
vibration frequency of the envelope had been reached. Therefore a small
test was made to determine the vibration frequency of the envelope and how
it vibrated under the impulse from an actual discharge. A light short
piece of thin wall stainless steel tubing was lightly compressed between
the lamp envelope surface and the center of a small audio speaker. The
voltage developed across an 1.1 kΩ resistor by the speaker movements was
then monitored with an oscilloscope. When the lamp envelope was tapped
sharply with a hard object a definite ringing frequency of 833 Hz could
sometimes be observed. This is shown in Fig. 6a. Figure 6b shows the
envelope vibration with an 80 J flashlamp discharge. In order to produce
a large build up in the vibration amplitude near 100 Hz PRF, the vibrations
would have to be re-enforced in a coherent manner every 10 msec. This
seems unlikely from the vibration waveform shown in Fig. 6b.

It was found that the vibration of the lamp deteriorates the porcelain
cement that bonds the aluminum end rings to the lamp envelope. A fine powder
and sometimes small chips of the cement are observed after several minutes
operation of the lamp. In a couple instances the end rings came loose
after about 10 minutes of operation. Thin lead seals have recenlty been
used with some success. After a minute run at 10 kW, however, the ends of
the envelope becomes hot enough to soften and partially melt the seals.
A water cooling jacket has just recently been installed that surrounds
the lamp envelope. The additional mass of the extra fused quartz jacket
and the water that fills the gap of about 2.5 mm between the jacket and
envelope should absorb the shock from the discharge much more readily
than the single envelope and help eliminate any vibration problems.

3.4 Optical Measurements on Flashlamp

The spectral irradiance of the flashlamp was measured with a $\frac{1}{4}$ meter
monochromator and photomultiplier. A quartz diffuser plate was placed
just ahead of the entrance slit on the monochromator to allow a uniform
illumination of the grating and photocathode. This system was carefully
calibrated using two quartz iodine standard lamps. The monochromator
was placed so that the diffuser plate was 1 meter from the axis of the
flashlamp. The flashlamp arc was then completely blocked except for a
1mm section at about the middle of the arc. By measuring the voltage
produced across a resistor by the photodetector current, we could determine
the peak spectral irradiance of the flashlamp at chosen wavelengths from
the uv to the red. As an example, Fig. 7 shows two simultaneous traces
one of the photomultiplier current and the other the flashlamp current.
The flashlamp current was measured using a Rogovski coil that was placed
around the return lead from the lamp housing. In this particular instance
the wavelength was set at 500 nm. The results are shown superimposed

FIG. 7

ARC CURRENT AND LIGHT OUTPUT FROM FLASH LAMP

---- 2 μf CAP, 150 J DISCHARGE, 12.25 kv

—— 4 μf CAP, 150 J DISCHARGE, 8.66 kv

N09-162-6

for both a 2μfd capacitor discharge and a 4μfd capacitor discharge. It is interesting to note that in each case the peak in the light output occurs approximately at the first zero crossing of the current. In addition, the current decays faster in one direction than in the other direction. It has been shown (Ref. 3 and 4) that for wall stabilized flashlamps the voltage and current relationship is given by

$$v = \pm K_o \left| i \right|^{\frac{1}{2}}$$

where the sign is chosen as the same sign as i. Using this non linearity in the circuit equation for the flashlamp, Markiewicz and Emmett (Ref. 5) computed the normalized current for different dampening parameters. Their results show a uniform dampening of the current for the underdamped case. Our current waveform does not agree with the above voltage and current relationship and with the results of Reference 5 probably because of the fact that the discharge is unconfined and expands outward releasing a shock front. This undoubtedly causes a different time variation in the arc plasma resistance than obtained in the wall stablized case. The shock front generation will be discussed in Section IV.

The peak irradiance measurements taken from the oscilloscope traces, were made at the monochromator calibration points from 250 nm to 700 nm. These measurements are shown by the points in Fig. 8. The spectral measurement indicates a continuous radiation at the visable wavelengths and probably some line emission in the uv. To compare these results with a black body radiation that has the same dimensions as the flashlamp arc we must calculate the radiance (N_λ) in terms of the irraciance (H_λ). This is givey by

$$H_\lambda = \int\limits_{\text{arc surface}} N_\lambda \Omega \cos\theta \, dA \approx N_\lambda \ell d / R^2$$

where Ω is the solid angle to 1 cm^2 at the detector, 1 the arc length, d the arc diameter, and R the distance from the arc to the detector. The approximations use the fact that $R \gg d$ and 1. For an equivalent blackbody source

$$N_\lambda = 1.19 \times 10^{-19} / \lambda^5 \left\{ \exp(1.438/\lambda T) - 1. \right\}$$

in units of watts/ster-cm^2-nm.

Then,

$$H_\lambda = 8.34 \times 10^{-25} / \lambda^5 \left\{ \exp(1.438/\lambda T) - 1 \right\}$$

in units of watts/cm^2-nm for the blackbody. The solid line curve in Fig. 8 gives the results of the above formula for H_λ with $T = 24,540°K$. This temperature

IRRADIANCE FOR 1 MM OF ARC LENGTH MEASURED 1 METER FROM ARC
AXIS WITH 150 J DISCHARGE INTO 6 CM GAP

then, approximates the radiating plasma temperatures in the arc channel for a 150 J discharge.

To estimate the total output power from the lamp at its peak irradiance we take the area under the spectral irradiance curve (Fig. 8) and multiply by 60 mm to allow for the entire arc length. The peak light power generated by the lamp is then found by multiplying the later figure by the ratio of the solid angle from a cylindrical radiating surface (π^2) to the solid angle of 1 cm^2 at a 1 meter distance. Thus

$$P_{FL} = \pi^2 \cdot 10^4 \int H_\lambda d_\lambda \approx 6.2 \text{ MW}$$

The peak power discharged by the capacitor into the arc is estimated from the light pulse or current duration as 43 MW. The electrical to optical efficiency for the flashlamp is then $\eta_{FL} = 6.2 \text{ MW}/43 \text{ MW} = .14$ or 14%. It is interesting to compare the flashlamp total power with the total power that would be emitted by a 24,540°K blackbody.

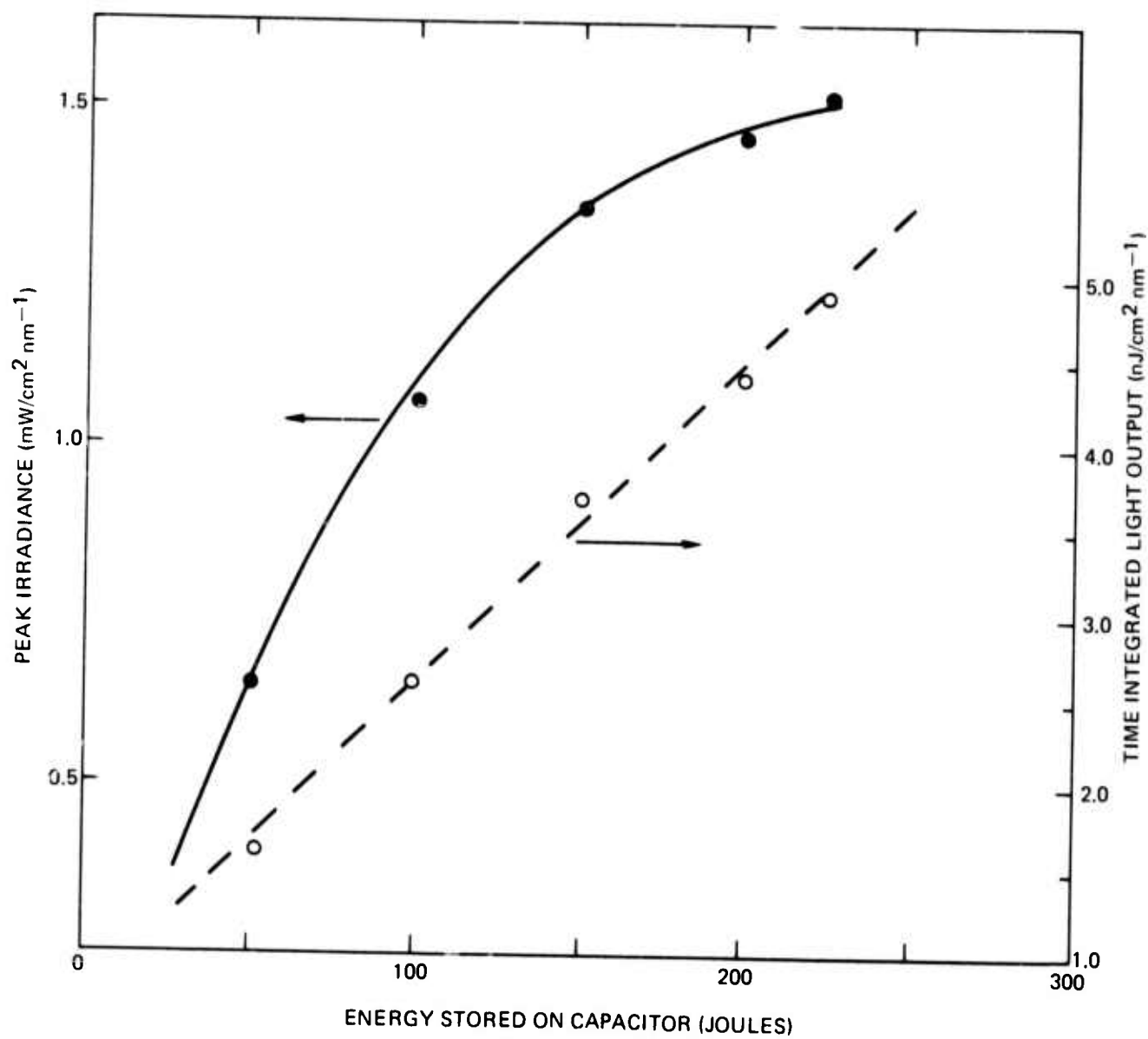$$P_{BB} = \pi^2 A \sigma T^4 / \pi = 84.7 \text{ MW}$$

where σ is the Stefan-Boltzmann constant and A the area of the lamp surface. This result shows that the discharge cannot possibly radiate as a blackbody over the entire spectrum.

Figure 9 shows a comparison of the optical power and energy output at 500 nm versus the energy discharged from a 2 μfd capacitor. From this result we see that the optical power begins to saturate at the higher input energies while the optical energy output continues to rise at a nearly linear rate. Therefore, the pulse duration is increasing at the higher input energies. Marshak (Ref. 3) shows similar data that demonstrates the saturation of optical power from an unbounded discharge for increasing input energy. Two possible explanations for this effect were given by Marshak. One explanation proposed the locking in of radiation at the higher input energies by an outside layer on the arc that has a high optical density. The other explanation which seemed more plasible was that the effective specific heat of the arc plasma increases at such a steep rate that further appreciable increase in T would call for an increase in energy concentration in the discharge, something difficult to attain in practice.

3.5 Temperature Measurements

A certain fraction of the power input to the lamp goes into increasing the internal energy of the gas. The power input that goes into internal energy can be determined by measuring the average temperature rise of the gas exiting from the anode. This temperature rise is created by the hot plasma
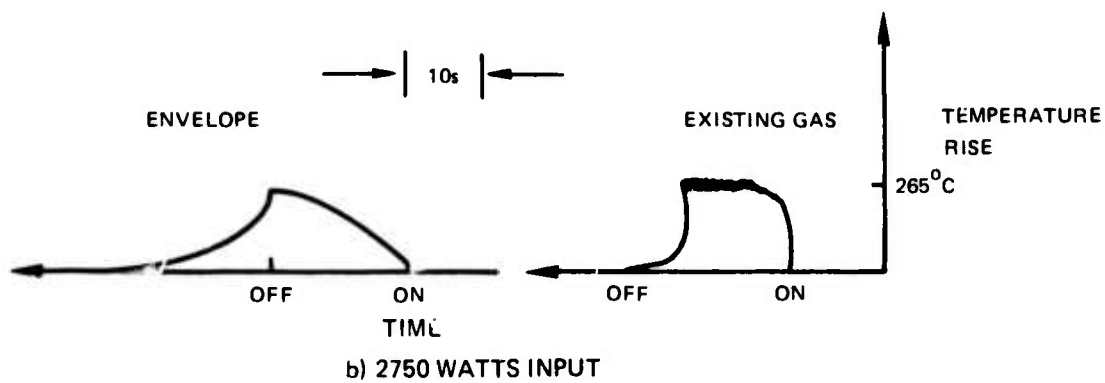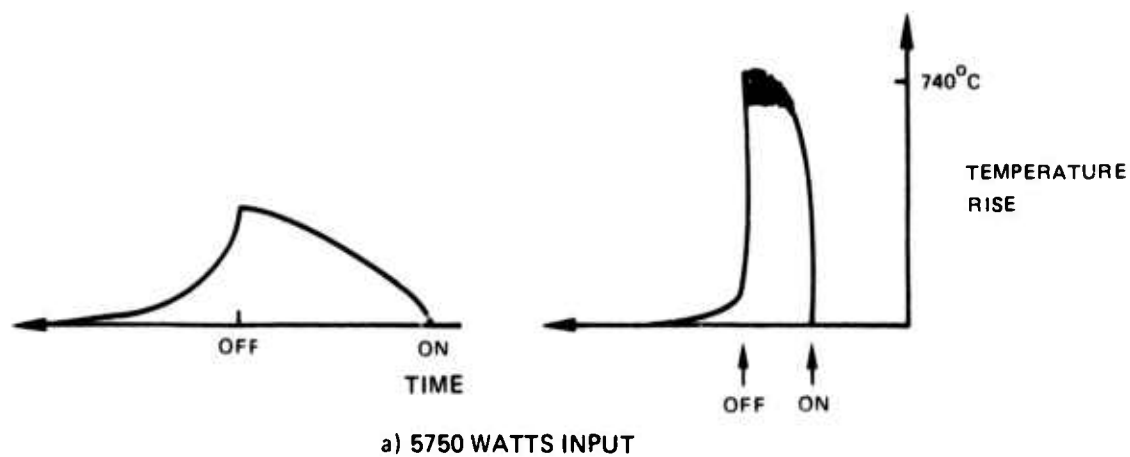
FIG. 9

FLASHLAMP OPTICAL POWER AND ENERGY VS INPUT ENERGY

generated during the electrical discharge and by the dissipation of the shock wave that is generated by the impulse of the discharge. The power that goes into internal energy in watts would be given by $E_{int} = 4.19 \, C_v \Delta T \, \dot{m}$. where C_v is the specific heat at constant volume, ΔT the temperature rise and $\dot{m}$ the mass flow of argon. Figure 10 shows the results of temperature measurements made on the gas at the anode and the temperature of the outside surface of the lamp envelope. The gas temperature was measured by insertion a 15 mil diameter calibrated thermocouple to a point just above the upper electrode gas outlet and about 1.8 cm from the arc. The input power level was set low at 5750 watts with a PRF of 115 Hz so as not to exceed the temperature measuring range of the thermocouple. The average temperature of the gas rose quickly to about 490°C during the first second of operation and then gradually stabilized to a temperature of 768°C after 15 seconds of operation. The temperature rise, then, was about 740°C and the power that goes into internal energy would be 2082 watts or 36% of the input power. The envelope temperature slowly increased to 393°C after 50 seconds of running. At 2750 watts input the gas temperature only went to 278°C as shown in Fig. 10b. The envelope, however, heated up to about the gas temperature after 36 seconds of running and has only a slightly slower rate of temperature rise than at the 5750 watt input level.

The approximately equal rate of temperature rise in Figs. 10a and 10b is inexplicable in view of the fact that energy is being put into the system over twice as fast in Fig. 10a (50J at 115 Hz) as compared to Fig. 10b (50 J at 55 Hz). To measure the envelope temperature a thermocouple was mechanically pressed against the outside wall. The wall vibration could have affected the measurement making the results for the envelope temperatures inaccurate. We can ascertain however from the rather slow temperature rise of the quartz envelope that convection cooling by the argon vortex flow is ineffective. As a consequence, the flashlamp has been modified as mentioned before to include a water cooling jacket that surrounds the lamp envelope. The water cooling should easily handle the heat loading on the fused quartz envelopes; offer more resistance to mechanical shock and vibration; and provide a means to optically filter the arc radiation. The importance of filtering the arc light was demonstrated recently on a laser similar to the one described in this report (Ref. 6). By inhibiting the shorter uv wavelengths from reaching the dye cell an increase the efficiency of the laser could be achieved under certain circumstances. In addition, removal of the infrared radiation could also help reduce the heat loading on the dye system which would help in repetition rate operation.

FLASH LAMP EXHAUST GAS AND ENVELOPE TEMPERATURE RISE

740°C

TEMPERATURE
RISE

OFF

ON

TIME

OFF   ON

a) 5750 WATTS INPUT

|← 10s →|

ENVELOPE

EXISTING GAS

TEMPERATURE
RISE

265°C

OFF

ON

TIME

OFF

ON

b) 2750 WATTS INPUT

- 23 -

SECTION IV

THEORY OF POWER DISTRIBUTION IN FLASHLAMP

4.1 Gasdynamics of Flashlamp Discharge

The electrical to optical efficiency of our vortex stablized flashlamp
which is an unconfined pulsed discharge with a duration (FWHM) of about 2μs,
was measured both calorimetrically (Ref. 7) and optically (cf. section 3.4)
to be about 13 to 15%. On the other hand, high power direct current arc
lamps are typically about 50% efficient in converting electrical input
to optical output (Ref. 8). Even well stablized pulsed arc discharges
of about 1 msec duration have demonstrated efficiencies of 64.8% (Ref. 9).
A major power loss in the dc arc lamp that accounts for a large part of
the remaining 50% of the electrical input is the heating of the electrodes
by large currents of several hundred amperes required for their operation.
The energy loss mechanism in the unconfined flashlamp, however, is considerably
different. Since the average currents for our lamp are on the order of 5A,
the electrode heating would represent only a small loss to the discharge
process. Indeed, when the flashlamp has been operating at 10 kW for a few
minutes and then suddenly turned off the electrodes are not even glowing
red hot. This is in contrast to the dc arc lamps. Whose red hot electrodes
contribute significantly to the heat loading of the lamps envelope by
infrared emission and absorption.

The major energy loss in the vortex flashlamp is in the creation of
a shock wave from the sudden release of energy and can be described qualitatively
in the following manner: at the onset a rapidly rising current density
in an initially small diameter arc channel creates a rapid rise in the
gas temperature which in turn increases the pressure in the arc channel
faster than the gas can expand to reach equilibrium with the surrounding
gas. The high pressure disturbance, driven further by the continued
heating of the discharge begins to move radially, outward and piles up
the gas molecules in a thin cylindrical region of very high pressure and
a sharply defined outside boundary. This pressure front or shock wave
continues to propagate outward faster than the speed of sound in the gas
and leaves behind in the luminous arc channel a region of low pressure.
The shock wave dissipates its energy and pressure as it moves outward
and eventually strikes the quartz envelope of the flashlamp producing a
large rap. In the luminous arc channel, which also expands outward but
not as fast as the shock front, the pressure is considerably below the
initial or undisturbed pressure.

The dynamics of a shock wave produced by the sudden release of energy
was treated by G. I. Taylor (Ref. 10) for the case of a spherical explosion
and then later by Shao-Chi Lin (Ref. 11) for the cylindrical case which

is applicable to our problem. For the gasdynamic analysis the authors used the equation of continuity, the equation of motion, and the adiabatic equation with the Rankine-Hugonoit relations for the gas conditions across a shock front. In addition, the assumptions were made that the ratio of the gas overpressure to the undisturbed pressure is much greater than unity; the gases behave as an ideal gas with constant specific heats; and the flow behind the shock wave is particle isentropic. For an instaneous release of energy E Lin obtains

$$R = 1.009 \ (E/\rho_o)^{\frac{1}{4}} \ t^{\frac{1}{2}}$$

where R is the radius of the advancing shock front, ρ_o is the undisturbed gas density, and t the time after the instantaneous release of energy E. Lin's results were also taken for a diatomic gas that has a specific heat ratio of 1.4. The radial velocity of the shock wave is given by

$$V = .505 \ (E_o/\rho_o)^{\frac{1}{4}} \ t^{-\frac{1}{2}}$$

and the pressure just behind the shock front is given by

$$P = .216 \ E/R^2$$

independent of the gas density. For an example, consider a 200 J discharge that occurs within 2μs in argon at 1 atm. The radius of the shock front at 2 μsec computed from the above equation would be 5.4 mm. Mack (Ref. 7) observed the time integrated luminous boundary to have a radius of about 4 mm for a 200 J discharge which is in reasonable agreement with the value for the radius of the shock front. The velocity of the shock fron at 2 μsec would be 1340 m/sec or 4.3 times the sound velocity. The pressure at the front would be about 14.5 atm. By the time the shock front reaches the lamp envelope at R = 1.7 cm the pressure would have dropped to 1.5 atm.

Using a more detailed analysis for an arc discharge, Drabkina (Ref. 12) has included the effects of the release of energy over a period of time rather than instantaneously.. She obtains for the shock front radius

$$R = (\alpha/\rho_o)^{\frac{1}{4}} \ \left[\int_o^t \ \{E(t)^{\frac{1}{2}} \} dt \right]^{\frac{1}{2}}$$

and for the shock front velocity

$$U = \frac{1}{2} \ (\alpha/\rho_o)^{\frac{1}{4}} \ \{ E(t) \}^{\frac{1}{2}} \ \left[\int_o^t \ \{ E(t) \}^{\frac{1}{2}} \ dt \right]^{-\frac{1}{2}}$$

where α is a dimensionless constant which depends only on the ratio of

specific heats and can be calculated from the energy integral. These
results are also discussed in the review article by Marshak (Ref. 3).
Drabkina also demonstrated that the outwardly progressing shock front
travels at a faster rate than the luminous boundary and, of course,
the two boundaries separate after a certain period of time. By defining
the luminous channel radius, $r(t)$, as the radius at which the gas
temperature falls to 10,000 K Drabkina shows that $r(t)$ is insensitive to
the actual temperature chosen to define the boundary and that

$$ r(t) = L \; \{E(t)\}^{m} \left[\int_{o}^{t} E(t)^{\frac{1}{2}} \; dt \right]^{N} $$

where for argon at 1 atm. $L = 1.1$, $m = .043$ and $N = .460$. If the energy
is supplied at a steady rate the luminous radius becomes

$$ r(t) = .91 \; \{E(t)\}^{273} \; t^{.46} $$

For a comparison, if we supply 200J of energy in 2 μsec, then, $r = 9.2$ mm
which is more than twice the radius observed in our flashlamp. Moreover,
Mack (Ref. 7) measured the radius of the luminous arc from photographs
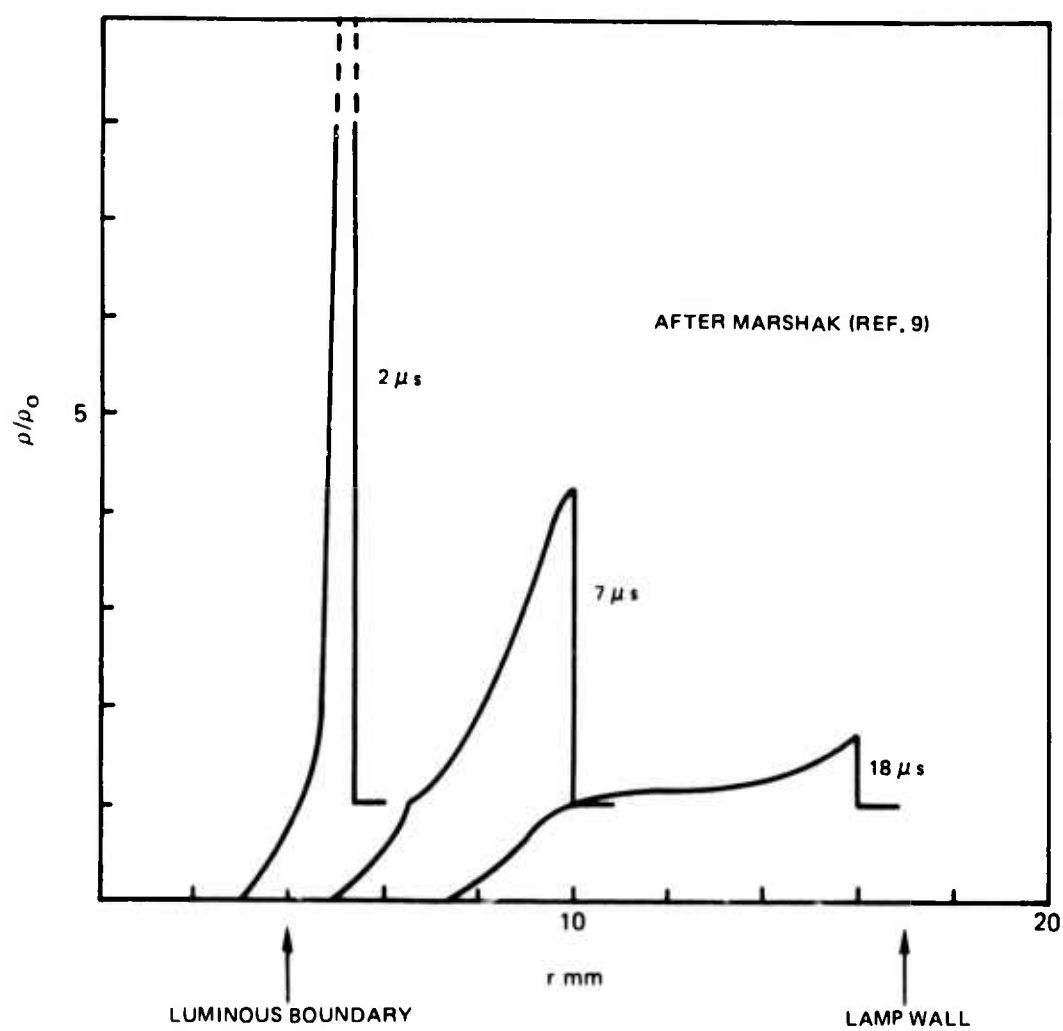as a function of the discharge energy to be given by

$$ r = AE^{x} $$

where A is a constant and x was between 0.43 and 0.76. Data collected
by Marshak (Ref. 3) from several different experiments and with different
gases indicates that a value of x between 0.4 and 0.5 describes the radius
of most systems. The theory, of course, is only approximate and does
not include important factors of how the energy is deposited in the dynamically
changing arc column.

Figure 11 shows how the density in an unbounded flahslamp might look
after a single discharge. The density distribution follows results presented
by Marshak (Ref. 3). The values placed on the graph correspond to what
would be expected from Lin's formulas, however. The knee on the inside
edge of the advancing shock front, referred to in Marshak's article as
a "sheath", was visable in sweep photographs using the Toepler shadow
method to make the regions of changing gas density visable. The sheath
region emits principally red and infrared radiation.

4.2 Thermodynamics of Gas Expansion in Flashlamp

Besides increasing the average temperature of the gas, by electrically
heating the plasma arc column, the flashlamp discharge performs mechanical

FIG. 11

SHOCK WAVE IN FLASH LAMP

AFTER MARSHAK (REF. 9)

$2 \mu s$

$7 \mu s$

$18 \mu s$

ρ/ρ_0

5

10

20

r mm

LUMINOUS BOUNDARY

LAMP WALL

-27-

work in expanding the gas. The **energy** that goes into gas expansion can be approximated by considering that the discharge energy is released instantly and that the temperature and pressure in the arc column rise at constant volume from the ambient conditions to the luminous arc temperature measured. The pressure reached at the maximum temperature would be obtained from the ideal gas law. The gas is then assumed to expand adiabatically since no additional heat energy can flow in or out of the gas in the time scale of the expansion. The constant volume pressure rise and consequent adiabatic expansion is shown by the broken line in the PV diagram in Fig. 12. The energy used to expand the gas would be the area under the broken curve (shown shaded in the figure). In reality since the discharge is not instantaneous, the gas does expand some during the deposition time of the electrical energy and consequently does **not** reach the peak pressures that would be predicted by the above assumption of a constant volume release of energy. The actual thermodynamic path on a PV diagram for average pressures and temperature might look something like that of the solid curve in Fig. 12. Using the original assumptions, the work done adiabatically in expanding the gas is
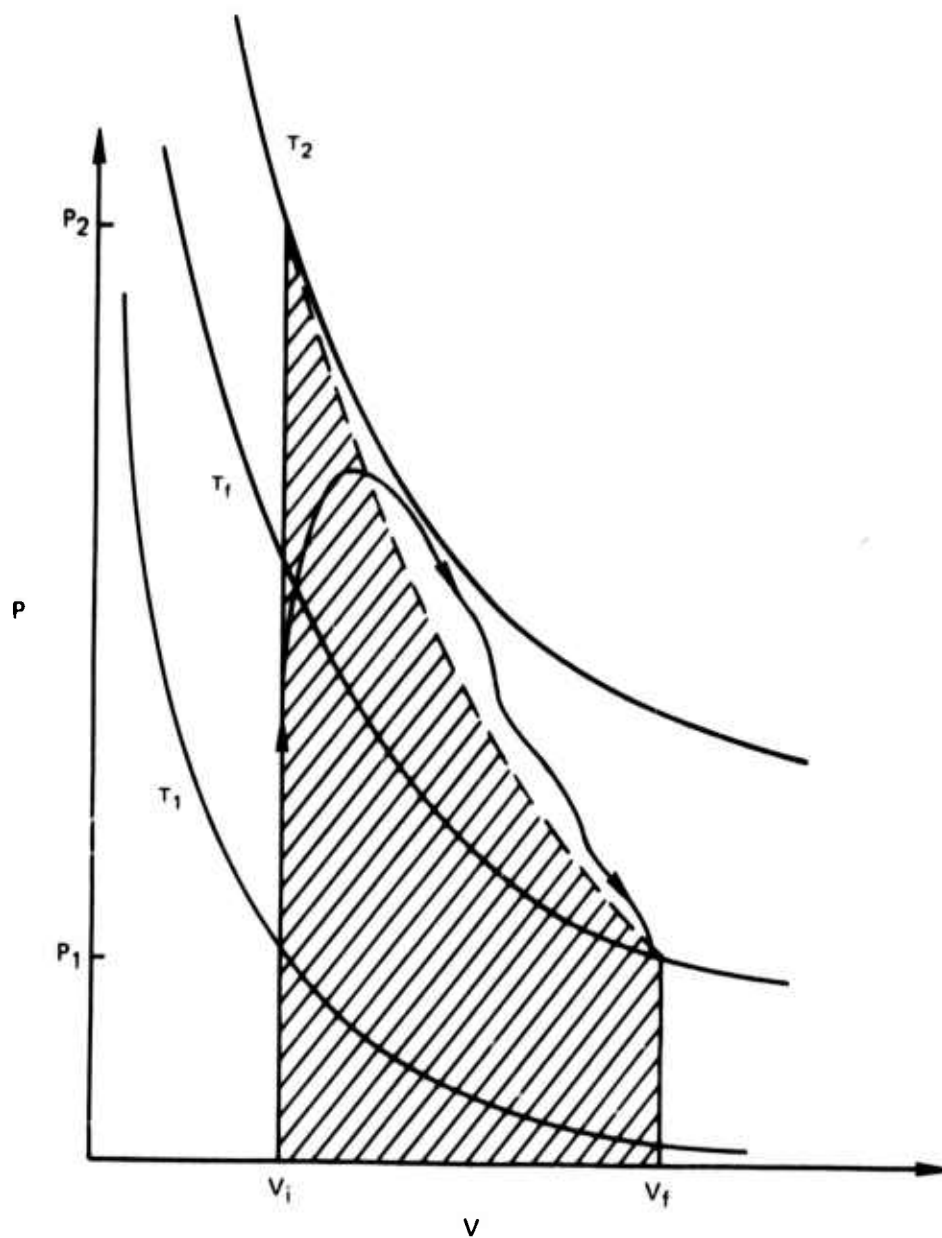
$$E_{exp} = \int P dV = c \int_{V_i}^{V_f} \rho \, V^{-\gamma} \, dV = \frac{c}{\gamma-1} (V_i^{-\gamma+1} - V_f^{-\gamma+1})$$

where c is the constant determined from the adiabatic law

$$P_2 V_i^\gamma = P_1 V_f^\gamma = c$$

$\gamma = 1.67$ for argon, $P_1 = 1.13$ atm. and $V_i = 2.53$ cm^3. From the ideal gas law $P_2 = nkT_2 = 64$ atm. where T_2 was taken to be 16,800°K for a 50 J discharge. The final volume and the constant c were then computed from the adiabatic law to be $V_f = 27.8$ cm^3, $c = 2.9 \times 10^{-3}$. We can therefore estimate the expansion energy as 18.8 J or 37.6% of the input energy. This expansion energy was based on a luminous arc diameter of .733 cm that was taken from a photographic negative. The actual luminous diameter is not exactly defined but the value chosen was an average value. Maximum and minimum values of the luminous diameter would have given about 48% to 26%, respectively, for the expansion energy.

FIG. 12

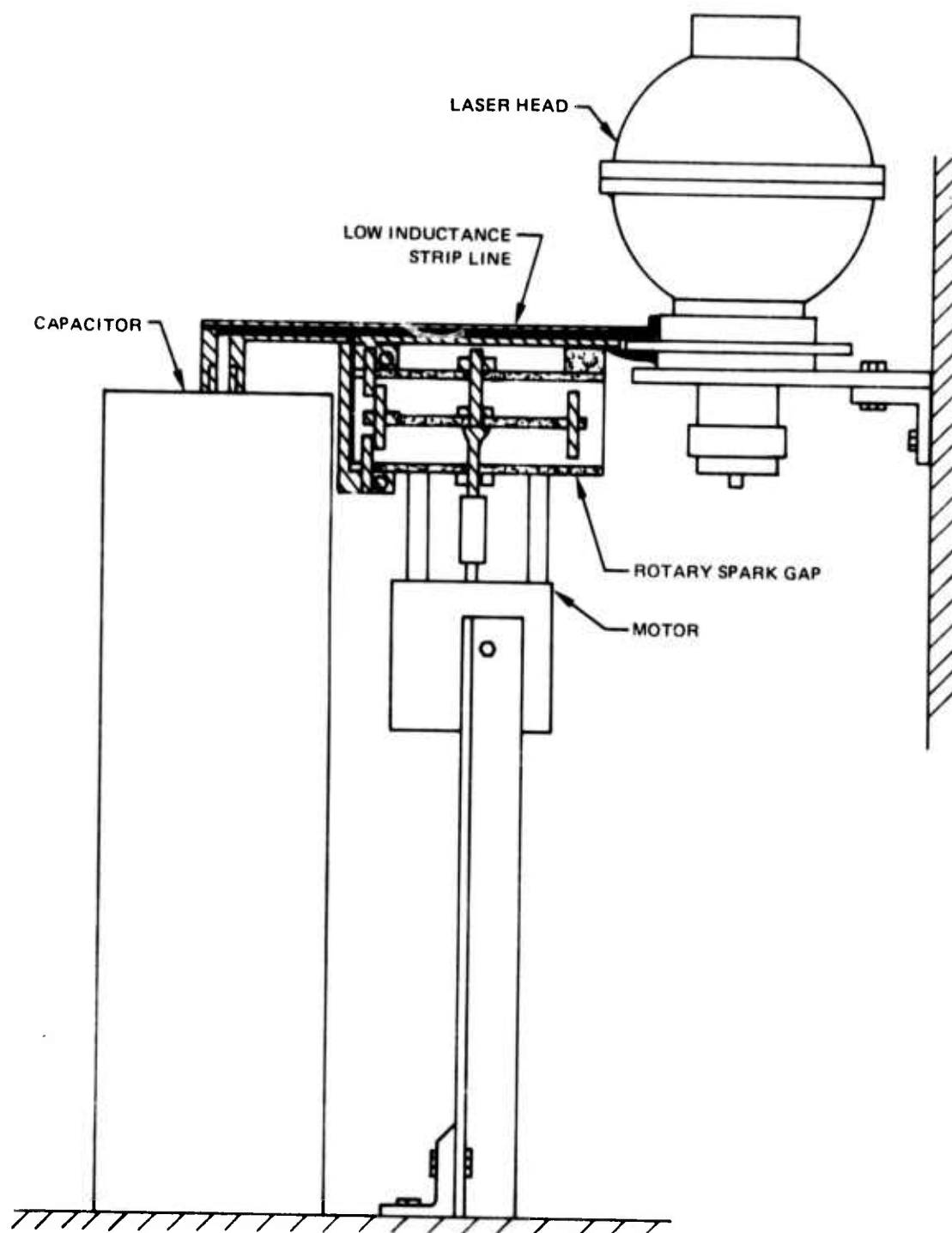## GAS EXPANSION IN FLASH LAMP

29-

SECTION V

ROTARY SPARK GAP

5.1 Design of the Rotary Gap

In the initial version of the flashlamp, the discharge was triggered
by a third trigger electrode that was inserted through the gas exit hole in
one of the electrodes. The main discharge was arranged to hold off the
desired firing voltage by the addition of a small admixture of CO_2,
(which incidentally increases the light output as well). A high voltage
pulse was applied to the trigger electrode to initiate the discharge.
This method of triggering is reasonably satisfactory for repetition rates
up to about 30 Hz. Beyond this point the residual ionization products
build up and lower the breakdown voltage of the main arc so that it is
no longer possible to discharge the desired energy per pulse. This problem
has been eliminated by the introduction of an external switch and a sustainer
discharge. The sustainer consists of a dc discharge of a few milliamperes
which is continually run between the lamp electrodes so that in effect the
arc is always broken down. When the lamp is to be fired, the switch to
the capacitor is closed and main discharge proceeds along the path of the
sustainer. This allows the discharge of any desired energy into the arc,
independent of the static breakdown voltage. The requirements on the switch
are rather stringent. It must be able to hold off 15-20 kV, switch 15 kA and
operate at several hundred Hz. In addition, it must have low inductance
and low loss. A very convenient solution to this problem was found in a
rotary spark gap. This type of switch was used in early radar transmitters.
A gap between two tungsten electrodes is repetitively bridged by a third
tungsten electrode carried on a rapidly rotating disc. Such a structure can
be incorporated into a low inductance stripline and does not significantly
contribute to the overall inductance. The rotary gap has been operated in
conjunction with the flashlamp at repetition rates up to 500 Hz and there
appears to be no reason why such a gap cannot be operated at rates up to
a few kHz. It would, of course, be possible to use a high power thyratron
in place of the rotary gap. Such thyratrons are near state of the art,
however, they are considerably more expensive than a rotary gap, have
limited lifetime, and for the present application offer no significant
advantage.

Figure 13 shows a cross sectional schematic of the rotary spark gap
and the manner in which it connects with the discharging capacitor and
laser assembly. The spark gap rotating disc that has four 5/16" diameter
by 2" long tungsten electrodes equally spaced and mounted on the circumference

FIG. 13

ROTARY SPARK GAP AND STRIP LINE ASSEMBLY

LASER HEAD

LOW INDUCTANCE STRIP LINE

CAPACITOR

ROTARY SPARK GAP

MOTOR

of the disc is shown in the center of the schematic. For convenience
sake the spark gap's disc or wheel was set to rotate in the horizontal
plane. The disc is rotated by a 1/2 hp router motor. A fiberglass-epoxy
material was used for the construction of the center of the disc and a
perforated aluminum annulus that attaches to the rim of the epoxy board
disc supports the electrodes. This construction allows for better heat
removal at the electrodes and electrical insulation of the connecting
shaft to the motor. There is an additional insulating spacer, however,
between the disc shaft and the motor shaft. The fixed electrodes were
originally mounted to epoxy board plates that formed the sides of the
supporting box for the rotating disc. The epoxy board was damaged by the
heat and intense uv light in the vicinity of the sparking electrodes
after several minutes of operation. As a consequence, the epoxy board
was replaced by a ceramic material that can withstand the environment
near the electrodes. A low inductance stripline made from heavy copper
strips and a 10 mil spacer sheet of overlaping mylan for insulation,
connects the capacitor, spark gap, and lamp housing. This is shown in Fig.
13. The top line, which is grounded runs directly from the capacitor to
the upper section of the lamp housing. The lower line, which runs from the
"hot" side of the capacitor to the lower part of the lamp housing is
broken by the spark gap. The capacitor side connects to the lower fixed
electrode in the spark gap and the lamp side connects to the upper electrode.
The rotating disc brings the moving electrodes in close proximity to the
fixed electrodes so as to bridge the gap between the two fixed electrodes
as shown in the figure. Aluminum blocks to which the fixed electrodes
are attached are cooled with circulating, deionized water from the flashlamp
cooling system. In addition, two jets of air are directed at the position
where the rotating electrodes come in close proximity to the fixed electrodes.
The flowing air helps remove the heat and residual ions from the sparking
region.

5.2 Electrode Wear

After an accumulated running time of about 10 minutes the spark gap
was disassembled and examined. It was found that both the fixed and moving
electrodes had visably worn at the positions where the sparking occured.
The two fixed electrodes were then weighed before reassembly of the spark
gap. A record was kept of the running time of the flashlamp in the succeeding
test runs. After an accumulated running time of 14.6 min with power inputs
ranging from 3.2 kW to 16 kW (8.8 kW average) the fixed spark gap electrodes
were removed and reweighed. It was found that the anode lost .342 grams
or .8% of its mass while the cathode lost .446 grams or 1% of its mass.
This corresponds to 1.4 and 1.8 grams lost per hour of running time.
Reports of electrode wear from rotary spark gaps used in early radars
indicate a much smaller rate of wear (Ref. 2). In the early radar spark
gaps the rate of cathode wear was considerably greater than the anode wear

and typical values of the wear rates in air were 3 to 4 mg per amp-hour
of current passed. These results were taken with pulse currents from 40
to 170 amp. The wear rate in nitrogen or gas mixtures that do not contain
oxygen was found to be 10 to 20 times greater and was attributed to the
oxygen forming a protective layer of tungsten oxide on the sparking surfaces.
The anode wear rates in air were only 1/5 that of the cathode wear rates.

The electrode wear mechanism for our spark gap must be different than
that in the early radar sets since the anode and cathode wear at approximately
the same rate; and the rate of wear expressed in grams per amp-hour is
0.75 g/amp-hour for the anode and .98 g/amp-hour for the cathode which is
more than two orders of magnitude greater than in the radar sets. The
pulse currents that we use, however, are two orders of magnitude greater
than those used for the radar gap measurements. On the other hand, the
electrode wear in the flashlamp has apparently been rather small even
after accumulated running times of about 30 minutes. Only a small amount
of wear appears around the exhaust holes in the center of the electrodes.
The considerably smaller rate of erosion from the flashlamp electrodes
as compared to the spark gap electrodes is probably due to the more effective
water cooling applied to the flashlamp electrodes. In the flashlamp, water
is brought to within a centimeter of the outside surface of the tungsten
cathode and 1.6 cm for the cathode. This greatly reduced the average
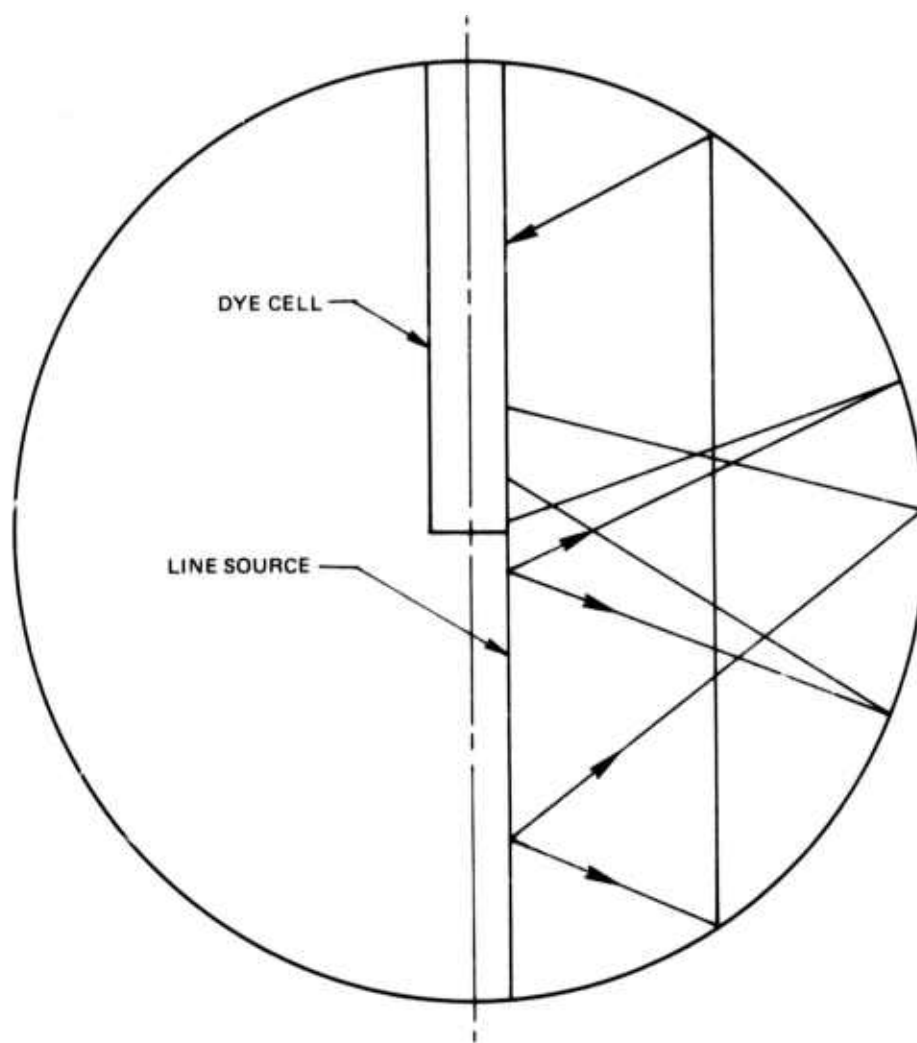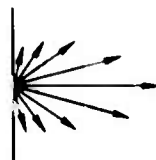surface temperature and extends the life of the electrodes.

SECTION VI

RAY TRACING PROGRAM

A computer program has been developed to calculate the efficiency of the laser pumping cavity and to determine the distribution of energy within the dye cell. This program will provide a guide to optimize the dye cell and arc diameters. Knowledge of the energy distribution within the cell can be used to determine the thermo-optical distortion and the dye concentration can be adjusted for the best compromise between the power output and the thermal distortion.

An idealized model of the pumping cavity is shown in Fig. 14. The dye cell is located on the axis of the cavity. The arc is assumed to be cylindrical and it is assumed to radiate from its surface as a black body. The symmetry of this configuration allows a considerable simplification in the calculation of the ray paths from the arc to the dye cell. Because of the symmetry, the efficiency for the cylindrical arc is the same as that for a line source that is displaced off the axis by an amount equal to the arc radius. Rays from this line source can thus be calculated rather than rays from the entire arc. This greatly reduces the number of rays that must be traced to obtain an accurate measure of the efficiency. The line source will, of course, provide an extremely asymmetric illumination of the dye cell. If we compute the power deposited by the line source in a given annular region of the dye cell, however, we will obtain the same radial distribution as would be produced by the actual cylindrical arc. This is illustrated in Fig. 15 .
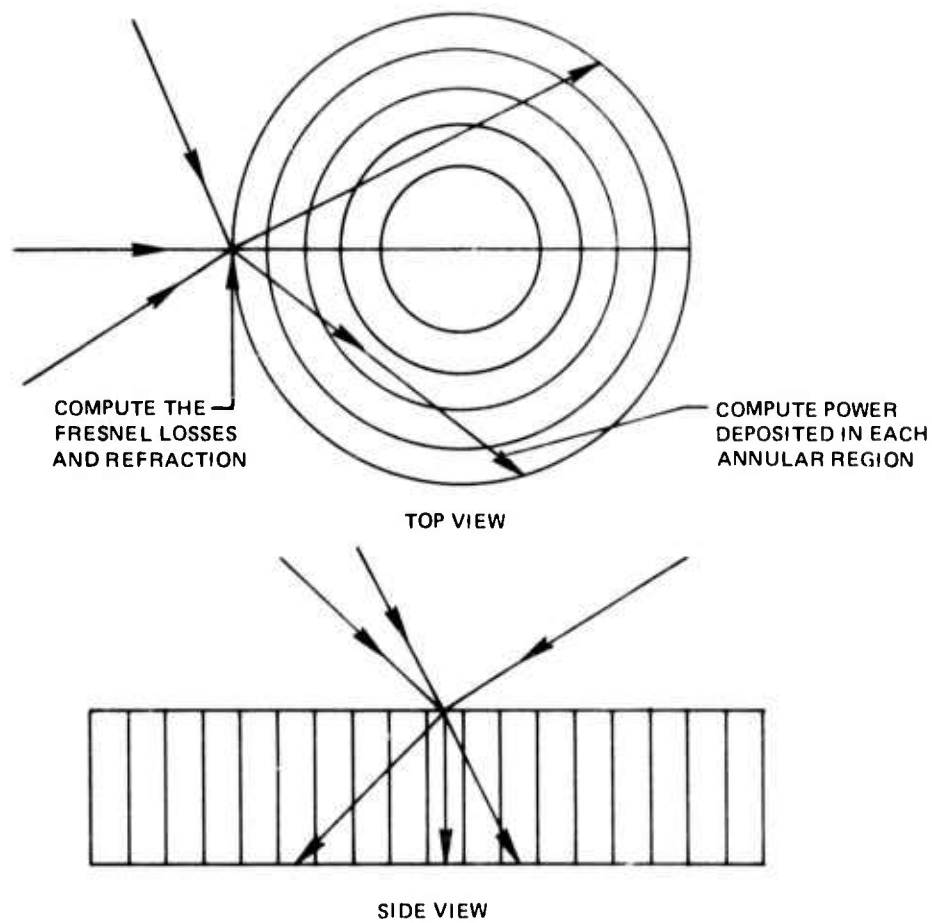
The computer program picks a number of points along the line source. From each point a bundle of rays is emitted with a Lambertian intensity distribution as shown in Fig. 14. The trajectory of each of the rays is traced, accounting for the losses on reflection from the sphere. Each ray is followed until it either hits the dye cell, the arc (where it is assumed to be reabsorbed) or decays below a specified intensity by multiple reflections from the sphere. If the ray hits the cell, the Fresnel losses are calculated and the direction cosines of the ray after refraction into the cell are computed. The trajectory of the ray is then traced within the dye cell and the power deposited in each annular region and axial region of the cell is computed. This process if repeated for the desired number of points along the line source and results in the determination of the power deposited in the cell as a function of r and z in the cell. The lengths and radii of the arc and dye cell are inputs to the program and may be chosen at will.

IDEALIZED CAVITY MODEL

DYE CELL

LINE SOURCE

TOP VIEW OF
LINE SOURCE

SIDE VIEW OF
LINE SOURCE

LAMBERTIAN EMISSION

-35-

POWER DEPOSITION IN CELL

COMPUTE THE
FRESNEL LOSSES
AND REFRACTION

COMPUTE POWER
DEPOSITED IN EACH
ANNULAR REGION

TOP VIEW

SIDE VIEW

Typical results for the efficiency are shown in Fig.   . In this case, the arc radius was held fixed at 3mm and the radius of the dye cell was varied. The efficiency initially increases with the dye cell radius and levels off, as one would expect, at a value approximately equal to the arc radius. In this case it was assumed that all rays incident upon the cell were absorbed.

From the efficiency, we may compute the optimum dye cell diameter. Initially, we will simplify the problem by assuming that the energy deposition wihin the dye cell is uniform. The gain coefficient of the laser, α, will then be proportional to the pumping power per unit volume, i.e.

$$\alpha \quad = \quad cp$$

where p is the pumping power density and c is a constant of proportionality. The gain of the laser will be

$$e^{\dfrac{\alpha}{1 + I/I_s}\,\ell}$$

where I_s is the saturation intensity and   is the length.   When the laser is oscillating, the gain must equal the loss, i.e.
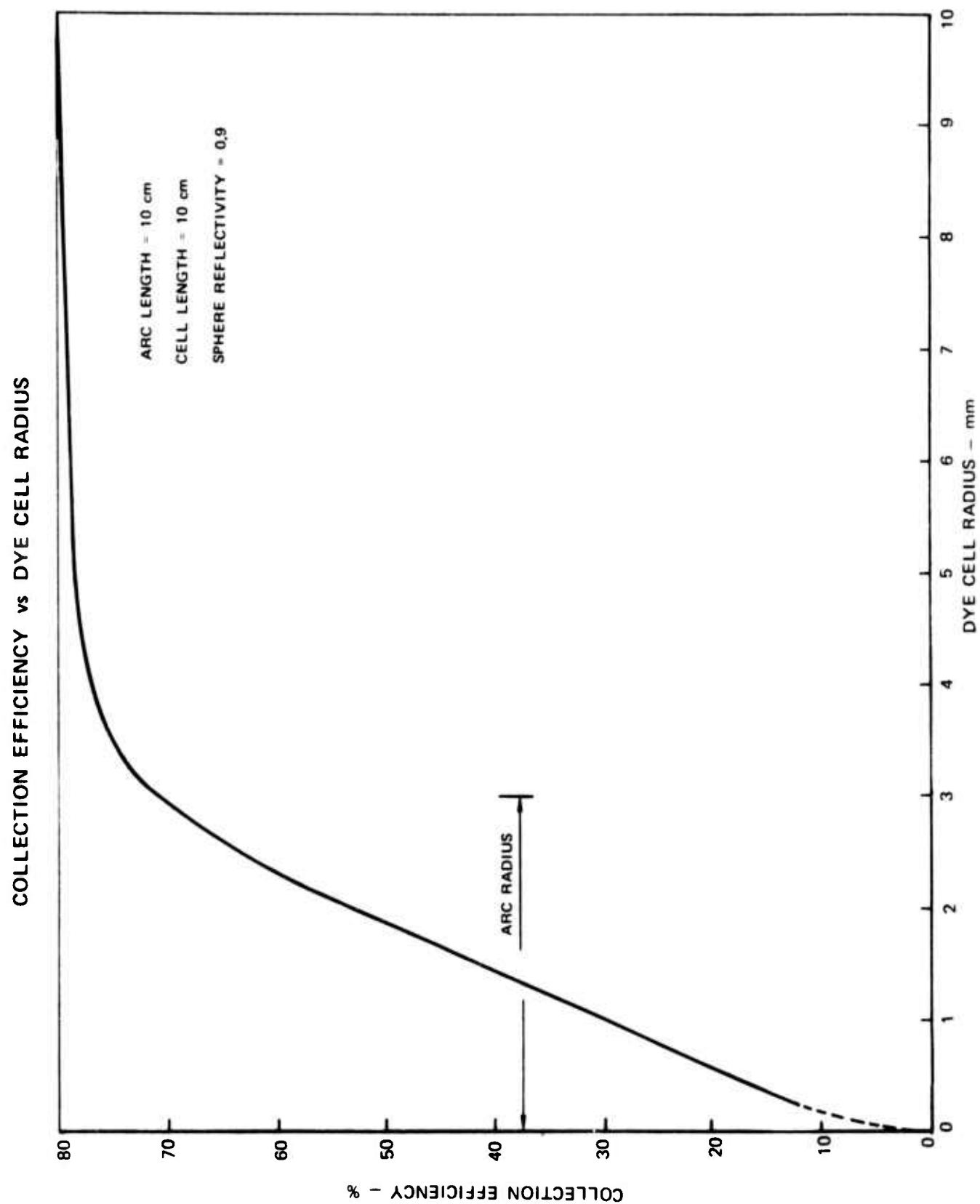
$$e^{\dfrac{\alpha \ell}{1 + I/I_s}}\; R_1 R_2 \;=\; 1$$

or

$$\frac{\alpha \ell}{1 + I/I_s} \;+\; \log\; R_1 R_2 \;=\; 0$$

The output intensity is thus

$$I \;=\; T\,I_s\left[-\frac{\alpha \ell}{\log R_1 R_2} \;-1\right]$$

Where T is the transmission of the output mirror. The total power out is the intensity times the area A of the beam

$$P_{OUT} \;=\; T\,I_s\left[-\frac{\alpha \ell}{\log R_1 R_2}\,A \;-A\right]$$

FIG. 16

COLLECTION EFFICIENCY vs DYE CELL RADIUS

ARC LENGTH = 10 cm

CELL LENGTH = 10 cm

SPHERE REFLECTIVITY = 0.9

ARC RADIUS

DYE CELL RADIUS — mm

COLLECTION EFFICIENCY — %

Since

$$\alpha = cp,$$

$$\alpha \ell A = \alpha v = cpv = cP_{pump}$$

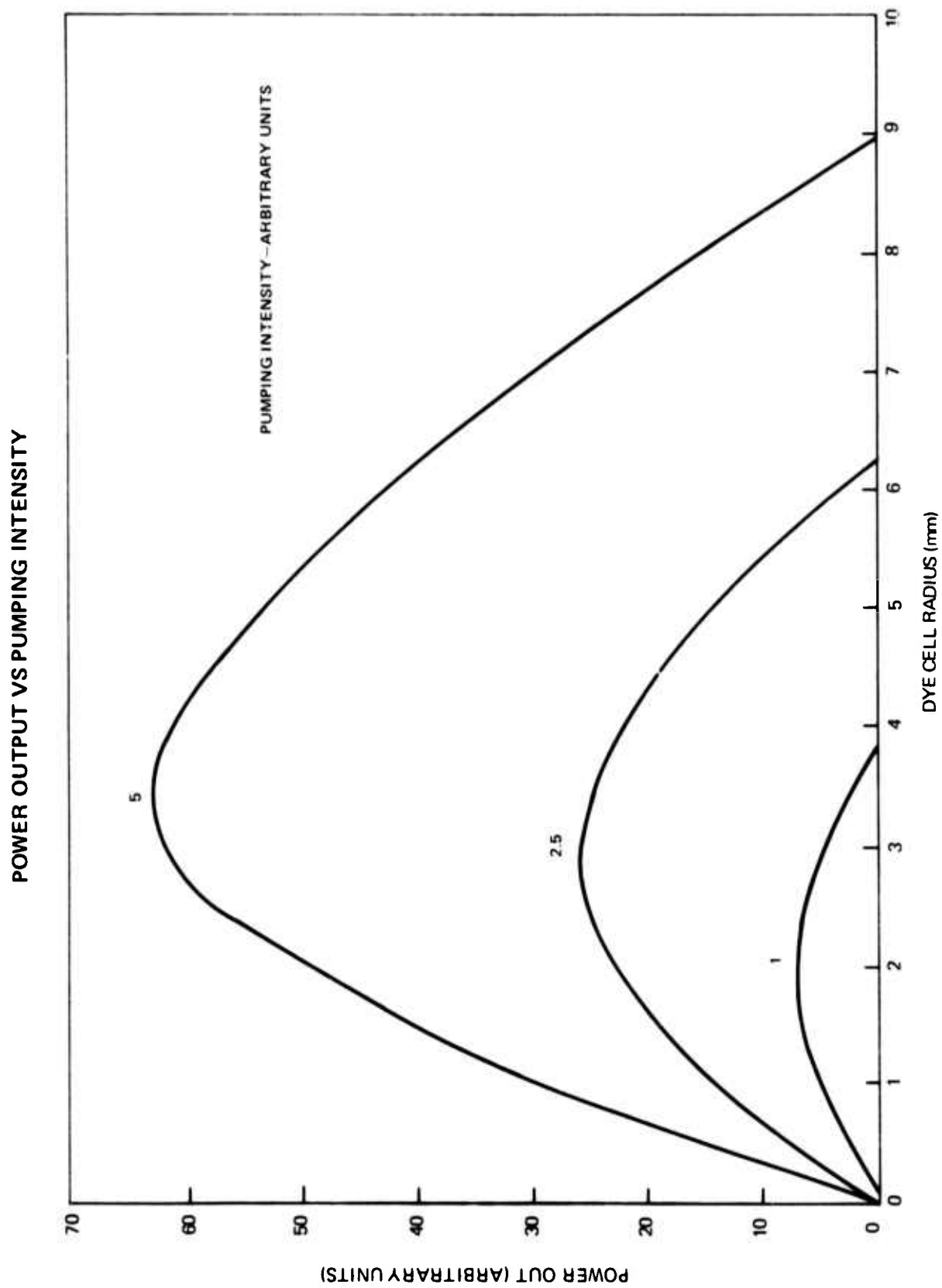i.e. $\alpha \ell A$ is proportional to the total pumping power. We have then

$$P_{OUT} = T\,I_s \left[-\frac{c\,P_{pump}}{\log R_1 R_2} - \pi\,r^2 \right]$$

$$= K \left[\beta\,P_{pump} - r^2 \right]$$

where K and β are constants of proportionality, $K = \pi\,T\,I_s$, $\beta = -c/(\pi \log R_1 R_2)$.
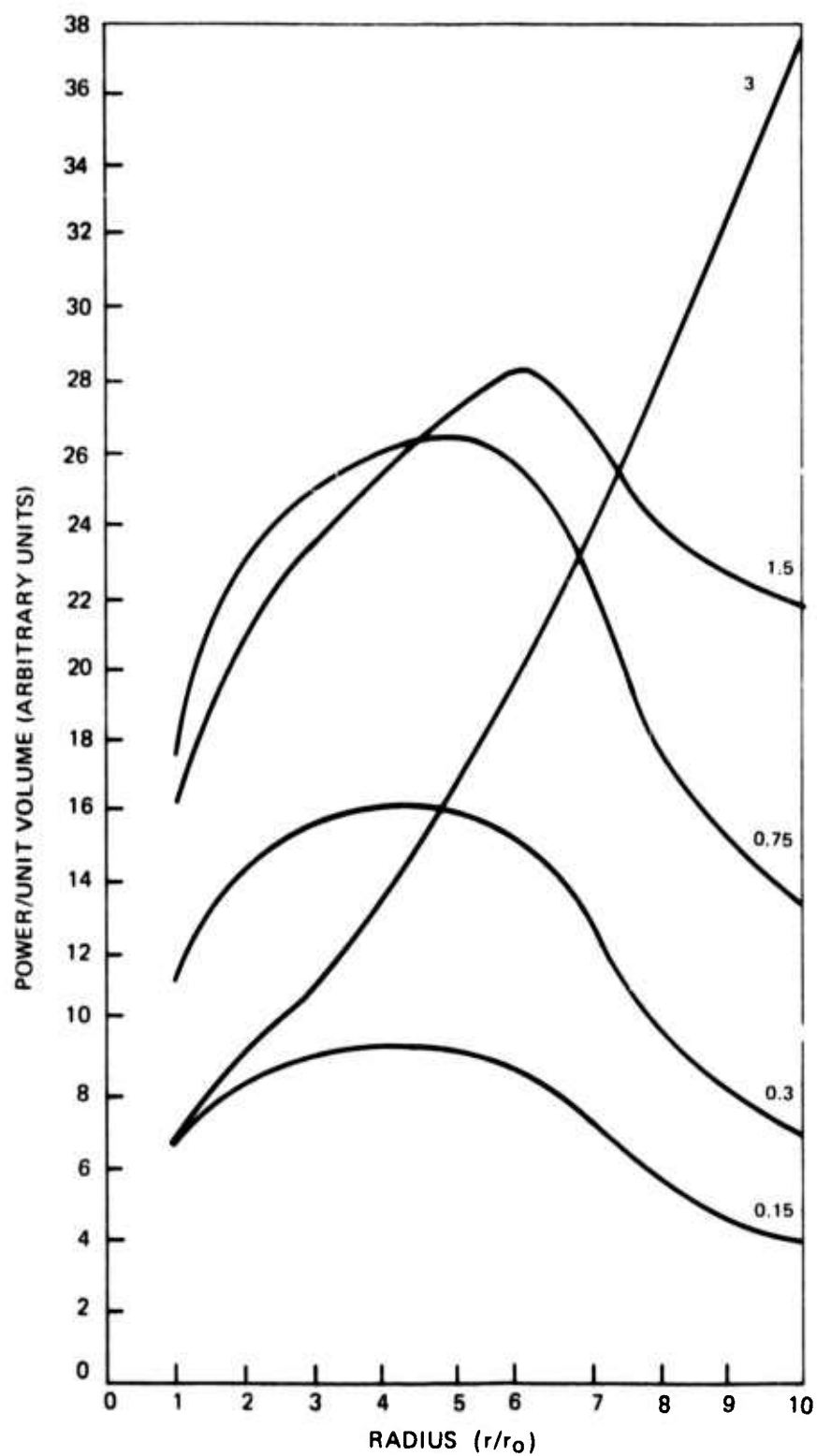
We may now plot the output power as a function of the pump power and the dye cell radius. Such a plot is shown in Fig. 17. These plots show that there is an optimum dye cell size and that this size increases with increasing pumping power (or correspondingly with decreased cavity loss or increased laser gain cross section). This is in agreement with experimental observations.

The pumping density is, of course non uniform and the computer program provides a detailed description of the pumping power density within the cell. An example of this is plotted in Fig. 18. The function plotted is the power per unit volume at a fixed axial position and the dye absorption coefficient is a parameter. In this case the dye cell radius and the arc diameter were both taken as 3 mm. The parameter on the curves is the number of absorption lengths in the dye cell radius, i.e. 3 corresponds to an attenuation of e^{-3} in transversing the cell radius. For low values of the absorption coefficient, a peak in the power distribution is observed within the cell. This is a result of the imaging of the arc. In the absence of the cell, the point on the arc would be imaged at the conjugate point in the sphere. For equal arc and dye cell radii, this would correspond to a point on the cell radius. Because of the refraction of the cell. However, it acts as a positive lens and images the arc at a point within the cell rather than at the radius of the cell. At higher dye absorption coefficients most of the power is absorbed at the outer edges of the cell before it can propagate to the image point.

This program, with suitable modifications and extensions will be

FIG. 17

POWER OUTPUT VS PUMPING INTENSITY

FIG. 18

POWER DISTRIBUTION IN DYE CELL

-41-

useful in optimizing the performance of both the present configuration and the transverse flow configuration discussed previously.

SECTION VII

DYE FLOW SYSTEM AND LASER POWER MEASUREMENTS

7.1 Dye Solution Pumping System

It was mentioned in Section I that a new, higher capacity, dye solution pumping system was assembled in order to increase the number of changes per second in the dye cell between flashlamp shots. This would help cool the cell walls and prevent the build up of thermo-optic distortion that reduces the laser power. The new pumping system consists of a 10 gallon per minute (GPM), series 36 liquiflow pump connected in parallel with a 20 GPM series 310 liquiflow pump. The pumps are of the rotating gear type and give a positive displacement output for an additive capacity. The importance of using a positive displacement pump was shown in separate tests (Ref. 6) that demonstrated that this type of pump gave far less cavitation than equivalent capcity centrifugal pumps. The pumps are driven with a variable speed 3 hp motor by way of a belt drive. An external graphite to ceramic seal was originally used to seal the pump shaft to the housing. This seal invariably leaked at pressures greater than 50 to 60 psig and the graphite wore down producing a fine carbon black power that eventually got into the system and clogged the filter. This caused an even greater pressure rise for a given flow rate. This seal was modified by using a tapered metal ring and "O" ring that was pressed against the ceramic material on the pump housing with the spring-loaded graphite piece. In this manner the graphite was kept out of the pump and slightly higher seal pressures could be maintained.

A large 22" long one μm Millipore filter is used to filter the output from the pumps. The filter besides removing small particulate matter acts principally as a site for the coalescense of tiny cavitation bubbles. These bubbles are continually generated by the pump and would remain in the solution for hours if it were not for the filter. One inch od by 7/8" id polyethelene tubing was used to connect the pumps, filter, and two reservoirs from which the dye cell input and output is taken. The two reservoirs and dye cell connections are shown in Fig. 1. The reservoirs with expansion bellows for pressurizing the system and coils for cooling the solution and the dye cell head (upper hemisphere) are essentially unchanged from the previous reporting periods (cf. Ref. 7) except for the addition of larger tube connectors on the reservoirs and larger id tubes in the dye head.

An 8 x 10 mm (id x od) size dye cell was used for the laser power test. The Reynolds numbe for the fluid flow at .63 ℓ/sec (10 GPM) is 75,000 and the flow is well into the turbulent regime. This is important because the turbulent flow will give better heat removal from the surface of the dye cell. The turbulent flow, however, requires more energy to drive
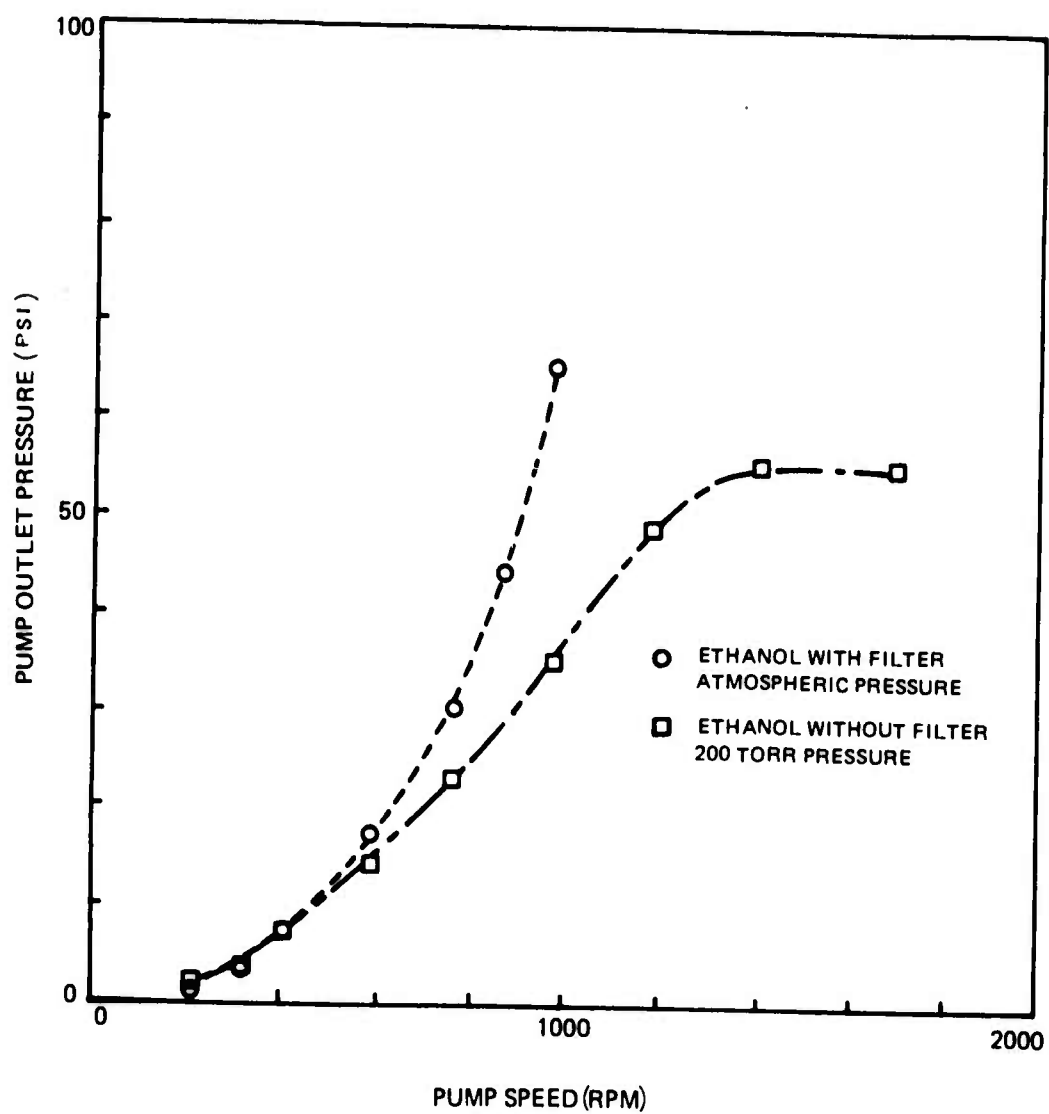
a given amount of solution through the cell and connecting tubes. The
pressure drop in a pipe with turbulent flow is approximately proportional
to the square of the average flow velocity ($\bar{v}$), the length of the pipe (L),
the density (ρ), and inversely proportional to the pipe diameter (D).
Thus,

$$\Delta P = f \, L \, \rho \, \bar{v}^2/2D,$$

where f the friction factor is a dimensionless constant of proportionality.
The friction factor is in general not constant but varies to some extent
with the Reynolds number of the flow and depends on the surface condition
of the pipe. Figure 19 shows a plot of the outlet pressure of the pump
versus the pump speed. For a positive displacement pump the pump speed
is proportional to the volume flow rate. For our system a maximum flow
rate of 1.89 ℓ/sec (30 GPM) would be reached at 1750 rpm. By the time we
reach a flow rate of 1.68 ℓ/sec, however, the pressure builds up past the
pump sealing capabilities. If we reduced the pressure on the dye system
with an aspirator we could reach a condition where the pressure would
saturate for increasing pump speed. This is shown in Fig. 19 with the dash-
dot curve and squre data points. In some instances when aspirating the dye
system we could even run at maximum rpm at a pressure of 20 psig. In these
instances, however, the pump is strongly cavitating and the volume flow rate
is no longer proportional to the pump speed. The pump seals, then, limit
the flow capacity for the present dye system. A sealless magnetic pump
could be used; but they are considerably less efficient and require a bigger
motor, are usually of the centrifugal type, and otherwise are rather
expensive. The largest pressure drop in the system occurs across the dye
laser head. If the flow conductance of the dye head could be increased the
pressure requirements would not be as great and allow an increase in the
flow rate with no leaking seals. In fact, the transverse flow system
discussed in Section II would have considerably more conductance than the
present system and permit the maximum flow rate to be attained with the present
pumping system.

Before the flow velocity that causes the pump seals to leak is
reached, however, a new problem emerges - cavitation in the laser dye cell.
The onset of cavitation in the dye cell is quite audible but barely visable
as distortions to the optical path along two opposite sides of the dye cell
near the right angle bends. The cavitation point is reached when increasing
the flow at a rate of about 0.45 ℓ/sec with atmospheric pressure on the
system. If the system is pressurized to about 20 psig, the cavitaion does
not start until about 0.63 ℓ/sec. After the initiation of cavitation, the
cavitation will persist for flow rates about 25% below the initiation flow
rate. The cavitation is barely visable as an optical distortion at the
onset, but the distortion increases in intensity and spreads out to cover
a greater percentage the dye cell cross section as the flow is increased
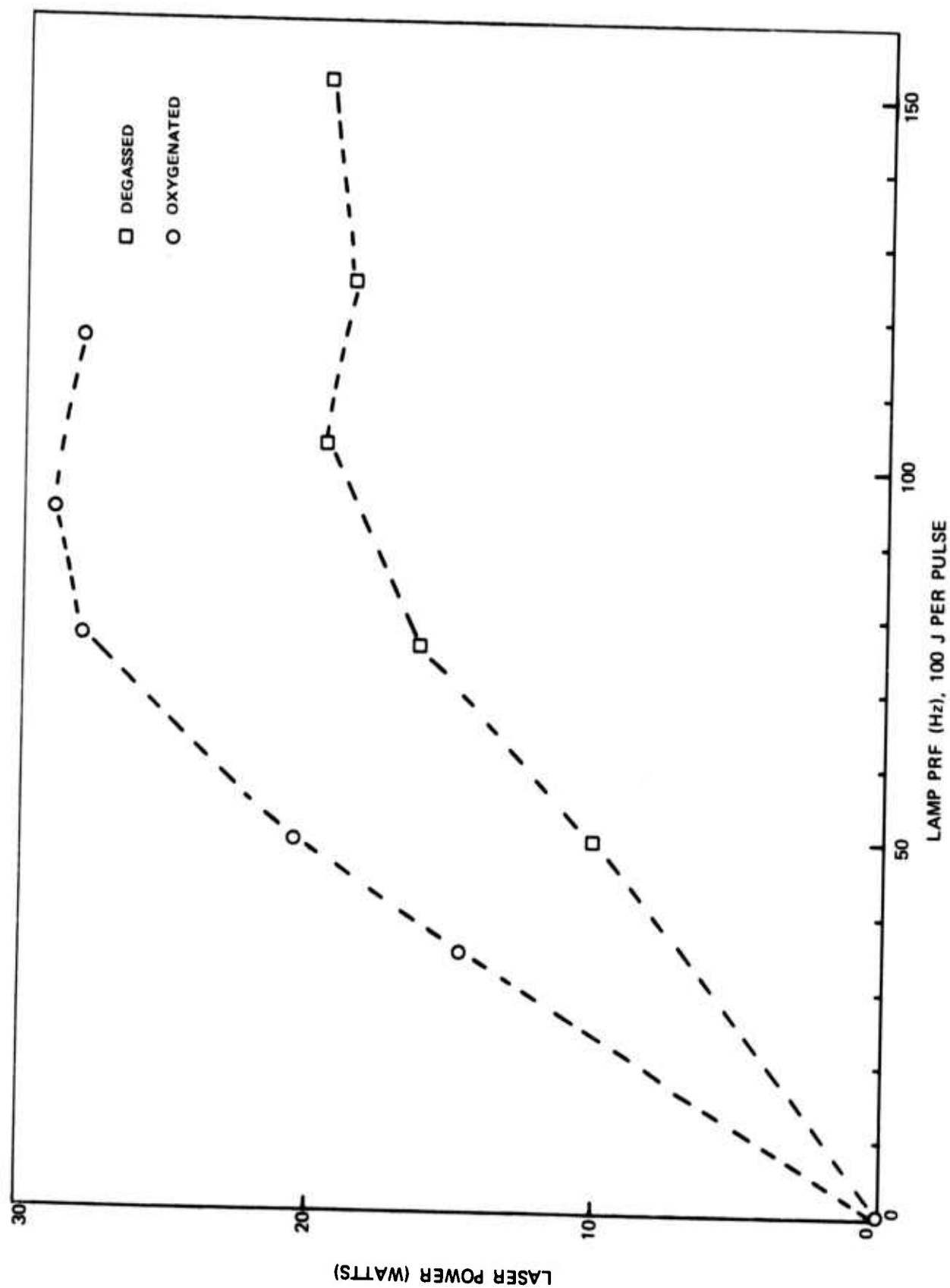
OUTLET PRESSURE VS PUMP SPEED

further. By the time the flow rate reaches pump seal limitations the distortion from the cavitation covers about 20% of the dye cell cross section.
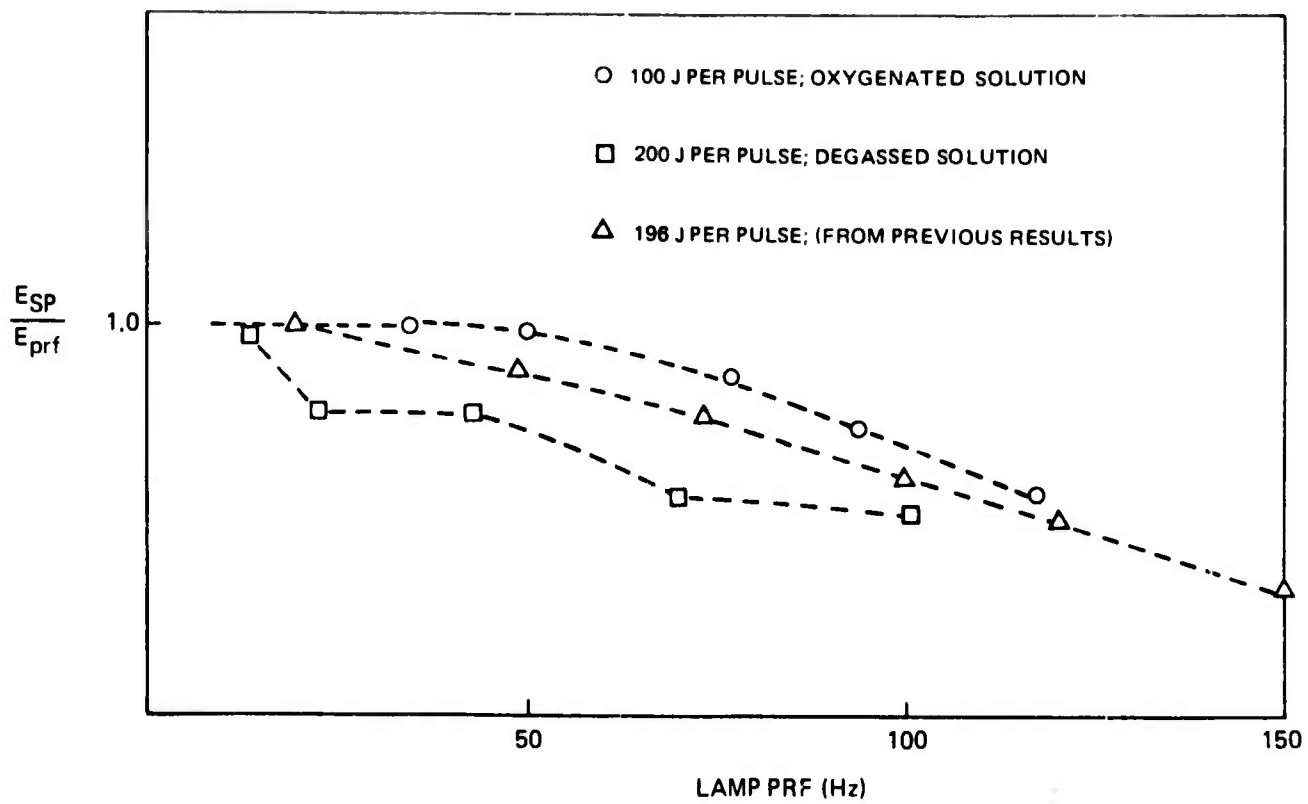
Instead of increasing the dye laser power as was indicated that we should do with the bigger capacity pumps, we found the limitations to the flow capacity in the present system first with the cavitation and then with the leaking pump seals. The cavitation problem may not be as serious as first thought; particularly, if it can be kept from the optical path by an improved hydrodynamic design. The pump sealing problem might be solved by the design of a seal to apply back pressure to the present seal or by redesign of the dye cell to allow a larger conductance as in the transverse flow system.

7.2 Laser Power Measurements

A series of laser output measurements were made with the new flashlamp and dye solution pumping system for both single shot energies and average power output at repetition rate operation. Rhodamine 6G tetrafloroborate dissolved in 200 proof ethanol at a concentration of 1.7×10^{-4} M was the solution used for the tests. The concentration had been optimized earlier on a similar but low repetition rate system (Ref. 6). Laser output coupling mirrors with reflectivities of 32%, 50%, and 65% were tried in the laser resonator. The 50% and 65% mirrors gave approximately the same results, but the 32% reflector gave about 26% less output energy. The 65% mirror was chosen for the laser power tests.

There was a significant difference in output between an oxygenated solution and a degassed solution. In fact, a 78% improvement was noted on the single shot energy output when oxygen was added at 1 atm. to a degassed solution. This improvement is due to the triplet quenching properties of oxygen in solution and has been discussed widely in the literature (Ref. 13). On a single pulse basis the electrical to laser energy efficiencies were: 0.42% at 100 J input, 0.39% at 150 J input, and 0.35% at 200 J input for an oxygenated solution with the 65% output reflector. The difference between the oxygenated and degassed solutions on the average power output is shown in Fig. 20. The oxygenated solution saturates at about 94 Hz while the degassed solution satruates at a slightly higher PRF of 103 Hz. The efficiency in rep. rate operation continues at about 0.4% up to 50 Hz and then slowly falls off due to thermal distortion. This result is shown more clearly in Fig. 2 where the ratio of the single pulse energy on a one shot basis to the single pulse energy at rep. rate operation is plotted verses lamp PRF. The circles in the Fig. 21 indicate data for 100 J per pulse input; the triangles indicate the results from the previous measurements on the old system; and the squares show the results from measurements taken on the new

FIG. 20

LAMP PRF (Hz), 100 J PER PULSE

LASER POWER (WATTS)

□ DEGASSED

○ OXYGENATED

$\dfrac{E_{SP}}{E_{prf}}$

O   100 J PER PULSE; OXYGENATED SOLUTION

□   200 J PER PULSE; DEGASSED SOLUTION

△   196 J PER PULSE; (FROM PREVIOUS RESULTS)

1.0

LAMP PRF (Hz)

50   100   150

system with 200 J per pulse input. It is believed that the data taken for
the 200 J per pulse result was hampered by a shorting problem in the spark gap.
In addition, allowance was not made in setting the power supply voltage
for the overvoltage swing on the capacitors as discussed in Section 3.2. The
actual energy per shot was more like 280 J which is an over rating of our
system.

It was interesting to observe the effects of cavitation on the laser
output. The energy per pulse on a single shot basis fell only 5% to 7%
even after the cavitation flow velocity had been exceeded by 65% for a degassed
solution. For an oxygenated solution the pulse energy fell about 15%
for the same flow conditions probably because of dissolved oxygen coming
out of solution in addition to vapor bubble formation from cavitation. For
rep. rate operation at constant input power the laser power reached a
maximum at a flow of 0.83 ℓ/sec for a degassed solution and 0.72 ℓ/sec for
an oxygenated solution. For faster flows the laser power decreased due to
the increasing optical distortion from cavitation and the release of dissolved
gases.

The research effort on the flow problems and on the optimization of
dye solutions or mixtures of solutons to use for high power operation has
just begun. At present the best output observed is 41 watts. When the
aforementioned problems have been investigated in more detail and more
experimental results are obtained, it is felt that the 41 watts will easily
be superseded. To obtain the low rep. rate efficiencies at high rep.
rate operation, however, may require a completely new dye cell design as
discussed in Section II.

REFERENCES

1. C. M. Ferrar "Rotary Spark Gap Switching For High Power Dye Lasers" Appl. Opt. 13, 1998 (1974)

2. "Pulse Generators" Dover Publication N. Y., N. Y. Ed. by Glasoe and Lebacqz

3. I. W. Marshak, "Strong Current Pulsed (Spark) Discharges in Gas, used in Pulsed Light Sources" Sov. Phys. Usp 5, 478 (1962).

4. J. H. Goncz, J. Appl. Phys. 36, 742 (1965).

5. J. P. Markiewicz and J. L. Emmett, "Design of Flashlamp Driving Circuits" IEEE, JQE QE-2, 707 (1966).

6. UARL Report AFAL TR-74-67 Dye Testing and Evaluation Program, Final Report under Contract F33615-73-C-1149, April 1974

7. UARL Report Number: M-921617-2, High Power Dye Lasers, Semi-Annual Technical Report 1 Jan 1973 to 30 June 1973. Sponsored under ARPA Order No. 1806

8. W. A. Jaatinen, E. A. Mayer, F. R. Sileo, "New Approaches to Sources For Solar Simulation" p 131 also Q. E. Lienhard "Compact Arc Lamps" p 145, International Symposium on Solar Radiation Simulation Proceedings, January 18-20, 19⁶⁶ Los Angeles, Calif.

9. J. H. Goncz and _. B. Newell "Spectrum of Pulsed and Continuous Xenon Discharges" JOSA 56, 87 (1966).

10. G. I. Taylor, Proc. Roy. Soc. (London) A201, 159 (1950).

11. Shao-Chi Lin, "Cylindrical Shock Waves Produced by Instantaneous Energy Release" J. Appl. Phys. 25, 54 (1954).

12. S. I. Drabkina, "Theory of the Development of the Channel of the Gas Discharge" JETP 21, 473 (1951).

13. J. B. Marling, D. W. Gregg, and S. J. Thomas "Effect of Oxygen on Flash-lamp-pumped Organic-Dye Lasers" IEEE JQE p 570 Sept. 1970.